



Distribution System Electromagnetic Modeling and Design for Enhanced Power Quality

Final Project Report

Power Systems Engineering Research Center

*A National Science Foundation
Industry/University Cooperative Research Center
since 1996*





Power Systems Engineering Research Center

Distribution System Electromagnetic Modeling and Design for Enhanced Power Quality

Final Project Report

Research Team Faculty

Sakis Meliopoulos, Georgia Institute of Technology
Elias Glytsis, Georgia Institute of Technology
George Cokkinides, Georgia Institute of Technology
Mladen Kezunovic, Texas A&M University

Research Team Students

Xi Zhu, Georgia Institute of Technology
Murad Asad, Georgia Institute of Technology
George Stefopoulos, Georgia Institute of Technology

PSERC Publication 05-14

April 2005

Information about this project

For information about this project contact:

A. P. Sakis Meliopoulos, Project Leader
Professor
School of Electrical and Computer Engineering
Georgia Institute of Technology
Atlanta, Georgia 30332
Phone: 404-894-2926
Fax: 404-894-4641
Email: sakis.meliopoulos@ece.gatech.edu

Power Systems Engineering Research Center

This is a project report from the Power Systems Engineering Research Center (PSERC). PSERC is a multi-university Center conducting research on challenges facing a restructuring electric power industry and educating the next generation of power engineers. More information about PSERC can be found at the Center's website: <http://www.pserc.edu>.

For additional information, contact:

Power Systems Engineering Research Center
Cornell University
428 Phillips Hall
Ithaca, New York 14853
Phone: 607-255-5601
Fax: 607-255-8871

Notice Concerning Copyright Material

PSERC members are given permission to copy without fee all or part of this publication for internal use if appropriate attribution is given to this document as the source material. This report is available for downloading from the PSERC website.

© 2004 Georgia Institute of Technology. All rights reserved.

Acknowledgements

The work described in this report was sponsored by the Power Systems Engineering Research Center (PSERC). We express our appreciation for the support provided by PSERC's industrial members and by the National Science Foundation under grant NSF EEC-0080012 received through the Industry / University Cooperative Research Center program.

We wish to thank all the PSERC members who provided support for this project, particularly the Steel Tube Institute of America.

Executive Summary

A new, comprehensive methodology for power quality assessment has been developed in this project. A key innovation is the use of physically-based models of electric power system components, coupled with Monte Carlo simulation to conduct the assessment. The models describe components by their physical characteristics and arrangements. From the physical descriptions, electrical models are derived while all constituent parts are explicitly represented. For example, steel conduit, neutral conductors, phase conductors (among other physical features) are explicitly modeled for a steel conduit enclosed circuit.

The overall power quality assessment model is efficiently solved in two steps. In the first step, the model is quadratized; that is, a nonlinear model of a system component is converted into a set of second order equations with the introduction of appropriate transformations. Then, in the second step, the quadratized model is solved with a Newton-type algorithm. The resulting analysis method is robust and efficient. This methodology can be used in time and frequency domain analyses.

The actual power quality assessment methodology is based on Monte Carlo simulation. As a result, it provides statistically-based assessment of power quality over different system conditions and events. The methodology predicts the expected performance of the system in terms of voltage sags and swells as well as with respect to published “susceptibility curves”.

The major results from this project include:

- A multiphase, secondary distribution system model for time domain and frequency domain analysis, including conduit enclosed power circuits.
- A comprehensive methodology for characterizing voltage sags and swells in power systems.
- A comprehensive methodology to assess power quality problems from a variety of transient phenomena including lightning.
- A comprehensive methodology that quantifies the effects of grounding system practices on power quality.
- A computer model for the statistical evaluation of any power system in terms of voltage sags and swells.
- An improved computer model for modeling permeable material conduit and enclosed power circuits, and for evaluating the mutual coupling between conduit enclosed power circuits and communication circuits.
- An integrated model of secondary power distribution networks with distributed energy resources. (This effort was also supported by CERTS.)

Table of Contents

<i>Acknowledgements</i>	<i>i</i>
<i>Executive Summary</i>	<i>ii</i>
1.0 Introduction	1
1.2 Main Accomplishments	2
1.3 Background on Power Quality Assessment	2
1.4 Summary Guide to this Report	3
2.0 Project Approach and Description	4
3.0 Model Development	5
3.1 Time Domain Analysis	5
3.2 Frequency Domain Analysis	7
3.3 Example Model: Generalized Conduit Enclosed Power Circuit	10
3.3.1 Modeling of General Conduit Enclosed Circuit – Magnetic Conduit	10
3.3.2 Finite Difference Implementation	17
4.0 Power Quality Assessment	19
4.1 Harmonics	19
4.2 Electromagnetic Fields	25
4.3 Voltage Sags and Swells	26
4.5 Asymmetry and Imbalance	30
4.6 Transients Propagation	31
4.7 Monte Carlo Simulation	33
5.0 Summary and Conclusions	38
6.0 Project-Related Publications	39
7.0 References	40
Appendix A: Computer Model Description	42
A.1 Computer Model GEMI	42
A.2 Computer Model μ GRID	47

Table of Figures

Figure 3.1. A General Conduit Enclosed Circuit.....	10
Figure 3.2. A Magnetic Conduit Enclosed Circuit	11
Figure 3.3. Relative Permeability versus Magnetic Field Intensity.....	12
Figure 3.4. Illustration of Conduit Segmentation into Slices.....	14
Figure 3.5. Detail of Segmentation and Notation for Difference Equations	15
Figure 4.1. Spectrum Analyzer Display of a Specific Voltage Waveform.....	20
Figure 4.2. Example Test System for Harmonic Resonance	21
Figure 4.3. Positive Sequence Harmonic Resonance – BUS70.....	22
Figure 4.4. Phase A to Neutral Resonance at BUS70.....	23
Figure 4.5. Example Test System for Harmonic Resonance	24
Figure 4.6. Positive Sequence Trans-Impedance (LOAD to BUS2)	25
Figure 4.7. Zero Sequence Trans-Impedance (LOAD to BUS2).....	25
Figure 4.8. Nomogram of Voltage Swells During Single Phase Faults.....	27
Figure 4.9. Distribution of Voltage Swells and Sags for a Specific Fault Condition and Circuit Design	28
Figure 4.10. Distribution of Voltage Swells and Sags for a Specific Fault Condition and Circuit Design – Deviation from Nominal, Voltages to Neutral	29
Figure 4.11. Distribution of Voltage Swells and Sags for a Specific Fault Condition and Circuit Design – Deviation from Nominal, Absolute Voltages	29
Figure 4.12. Example Distribution System for Unbalance Studies	30
Figure 4.13. Typical Results of Unbalance and Effects on Induction Motors.....	31
Figure 4.14. Time Domain Simulation of Transient Voltages.....	32
Figure 4.15. Disturbance Characterization Relative to the Susceptibility Curve	33
Figure 4.16. Probability Density Function of Voltages (Phase to Neutral) at BUS2	34
Figure 4.17. Probability Density Function of Voltages (Absolute Voltages) at BUS2	34
Figure 4.18. Disturbance Characterization Relative to the Susceptibility Curve	35
Figure 4.19. Statistical distribution of Disturbance Voltages Relative to the Susceptibility Curve.....	36
Figure A-1. GEMI Program Single Circuit Steel Conduit Analysis Mode	43
Figure A-2. GEMI Program Single Circuit Aluminum/PVC Analysis Mode.....	43
Figure A-3. GEMI Program Network Editor.....	44
Figure A-4. GEMI Program Data Entry Form for a Steel Conduit Enclosed Circuit.....	45
Figure A-5. GEMI Conduit Selection Window	45
Figure A-6. GEMI Cable Selection Window.....	46
Figure A-7. GEMI Program Magnetic Field Report Form for a Steel Conduit Enclosed Circuit.....	46
Figure A-8. GEMI Program Results Display View	47
Figure A-9. μ GRID Program Network Editor	48
Figure A-10. Microturbine Model Data Entry Form	49
Figure A-11. Multimeter Tool Displaying Microturbine Operating State.....	50

1.0 Introduction

This project is an effort to develop analysis and design tools for maximizing power quality of medium and low voltage power circuits without or with distributed energy sources. Specific focus areas are:

- Develop an understanding of the relationship between distribution system grounding and distribution system performance measured with (a) feeder outages, temporary interruptions, voltage sags and voltage swells, (b) power quality at the end user and (c) safety.
- Develop an understanding of the interaction of utility systems and the end user electric installations. Quantify the effects of design options in terms of EM fields, safety and interruptions.
- Identify needs for analysis methods to properly address these issues.
- Develop design guidelines for cost-effective power quality improvements.

Disturbances that affect power quality are multiple: (a) lightning, (b) switching, (c) power faults, (d) feeder energization inrush currents, (e) motor start, (f) load imbalance, (g) harmonics and resonance, and (h) EMI. The effects on the end user could be voltage distortion, voltage sags, voltage swells, outages, and voltage imbalance. These effects may have different levels of impact depending on the susceptibility of the end-user equipment. For a specific susceptibility of end-user equipment, the impact of disturbances can be mitigated by design modifications of circuit layout, grounding system design, overvoltage protection, filters, use of steel conduit, use of additional transformers, etc. Traditional power system analysis methods are based on models that do not capture these phenomena, for example, the most usual models of sequence components do not predict the voltages in neutrals or grounds and therefore are not appropriate for accurate prediction of voltage variations. This report proposes a new modeling approach and analysis method for better voltage disturbance evaluation. We address the steady state case as well as transient case.

The proposed method is based on modeling electric power system in their physical configuration (i.e., 3-wire, 4-wire or 5-wire system) without the use of any transformations, such as the symmetrical component transformation. We also propose a new analysis method for the overall electric power system based on physical models. The proposed methodology is capable of modeling systems with three phase wires, four wires (three phase and a neutral/or ground wire), five wires (three phase wires, neutral and a ground wire), single and double phase circuits, grounding and bonding points, and grounding systems. The proposed methodology has additional desirable features. For example, a physically based model can explicitly represent grounding systems, the size of the neutral wire, and the ground wires. These practices have been known to have great effect on power quality. Another important property is that a physically based model and analysis procedure provides the means to expose the interrelationship between the physical parameters and power quality. This property naturally leads to comprehensive cost-benefit analysis.

The report presents the proposed methodology and provides practical examples.

1.2 Main Accomplishments

The main accomplishments of this project are:

- Formulation of a multiphase secondary distribution system model for time domain and frequency domain analysis and including conduit enclosed power circuits.
- A comprehensive methodology for characterizing voltage sags and swells in power systems.
- A comprehensive methodology to assess power quality problems from a variety of transient phenomena including lightning.
- A comprehensive methodology that quantifies the effects of grounding system practices on power quality.
- A computer model for the statistical evaluation of any power system in terms of voltage sags and swells.
- An improved computer model for modeling permeable material conduit and enclosed power circuits and evaluating the mutual coupling between conduit enclosed power circuits and communication circuits.
- An integrated model of secondary power distribution networks with distributed energy resources (This particular effort was also supported by the Consortium for Electric Technology Solutions, described at <http://certs.lbl.gov/>).

1.3 Background on Power Quality Assessment

Disturbances that affect power quality include such phenomena as (a) lightning, (b) switching, (c) power faults, (d) feeder energization inrush currents, (e) motor start, (f) load imbalance, (g) harmonics and resonance, and (h) EMI. The effects on the end user could be voltage distortion, voltage sags, voltage swells, outages, voltage imbalance, among other effects. These effects may have different levels of impact depending on the susceptibility of the end-user equipment. For a specific susceptibility of end-user equipment, the impact of disturbances can be mitigated by design modifications of circuit layout, grounding system design, overvoltage protection, filters, use of steel conduit, use of additional transformers, and other design options. The effectiveness of these design options on power quality can be analyzed with specialized analysis software. The analysis methods should be able to model systems with three phase wires, four wires (three phase and a neutral/or ground wire), five wires (three phase wires, neutral and a ground wire), single and double phase circuits, grounding and bonding points, and grounding systems. Such comprehensive methods do not exist. The focus of the research of this project was to “fill the gap” by developing methodologies that address these issues.

1.4 Summary Guide to this Report

Section 2 provides a description of the research project objectives.

Section 3 describes the mathematical techniques used in the development of power system models. Specifically, time domain and frequency domain simulation methods are presented based on quadratized power system component models. The generalized model equations are described, as well as a detailed example model of a steel conduit enclosed power circuit.

Section 4 presents several applications of the developed methodology, including analysis of power system harmonics, electromagnetic fields generated by power circuits, voltage sags and swells due to faults, propagation of lightning induced transients via deterministic as well as Monte Carlo based methods.

Section 5 presents a summary and conclusions of the project research.

Appendices A and B provide brief descriptions of two computer models used in this project: GEMI and uGrid. The computer Model GEMI focuses on the analysis and design of power distribution systems containing steel conduit enclosed circuits, and in particular on the effects of the magnetic properties of the steel conduit in the performance of the distribution system. The computer model uGrid provides power flow analysis of power distribution networks containing distributed sources such as microturbines, fuel cells, inverters etc.

2.0 Project Approach and Description

The research objective is to develop methodologies that will allow systematic investigation of all known factors affecting power distribution system performance and connected end user electrical installations including distributed energy sources. These factors are: (1) lightning (direct and induced), (2) switching, (3) power faults, (4) feeder energization in-rush current, (5) loading imbalance, and (6) harmonics. For example, it is known that induced lightning may result in a power fault and subsequent voltage sag in one phase and over-voltage at the other two phases. The grounding system design plays an important role in (a) determining whether an induced lightning may result in a power fault in the first place and (b) the level of voltage sag and over-voltage. Thus, this approach will result in the characterization of the effects of these parameters on power quality.

The research has been focused on developing comprehensive analysis tools for evaluating the power quality performance of typical distribution systems as affected by the factors mentioned above. The performance of power distribution systems has been quantified with statistical measures of frequency and duration of the disturbances with respect to the CBEMA susceptibility curve. The basic analytical tool is a Monte Carlo simulation with effects analysis. The models have been exercised on several alternate system designs and overvoltage protection schemes. The results are summarized in this report. Conclusions are drawn as to the effectiveness of the various design practices in improving the performance of distribution systems.

The design practices for medium and low voltage systems are in general different in Europe and the United States. A collaborative effort with researchers in Europe has been focused on defining the differences. The results of these comparisons have been reported in technical papers that are listed in this report.

3.0 Model Development

This section describes the modeling approach and development. The modeling approach is based on methods that explicitly and accurately represent system asymmetries and imbalances. The modeling is “physically” based; i.e., it relates to the design parameters and geometry of the components (power lines, transformers, power electronic blocks, etc.). The implication is that system performance can be directly coupled to specific design parameters. This is an important advantage and to our knowledge, this approach is not used elsewhere.

Several representative components of electric power systems have been developed using the above mentioned approach. In particular, a generalized model of conduit enclosed power circuits has been developed. This model is an extension of the previous single conduit model that was developed in the program GEMI. The new model permits the evaluation of induction phenomena among power circuits enclosed in conduit. It accommodates frequency domain analysis and well as time domain analysis. In case of steel conduit, it models the saturation effects of the steel conduit. The model has been fully developed within the GEMI program.

The modeling methodology presented here has the capability to perform steady state (frequency domain) analysis and well as time domain analysis. These two analysis methods are based on a quadratized model of all power system components and use Newton’s method to obtain the network solution. A brief description of the method (both frequency domain and time domain) is presented in general form. Following this description, an example of component modeling is presented. The specific example used is a generalized model of conduit enclosed power circuit.

3.1 Time Domain Analysis

Any power system device is described with a set of algebraic-differential-integral equations. These equations are obtained directly from the physical construction of the device. It is always possible to cast these equations in the following general form:

$$\begin{bmatrix} g\left(\frac{di}{dt}, i\right) \\ 0 \end{bmatrix} = \begin{bmatrix} f_1\left(\frac{dv}{dt}, \frac{dy}{dt}, v, y, u\right) \\ f_2\left(\frac{dv}{dt}, \frac{dy}{dt}, v, y, u\right) \end{bmatrix} \quad (3.1)$$

where i : vector of terminal currents
 v : vector of terminal voltages
 y : vector of device internal state variables
 u : vector of independent controls.

Note that this form includes two sets of equations, which are named *external equations* and *internal equations* respectively. The terminal currents appear only in the external equations. Similarly, the device states consist of two sets: *external states* (i.e., terminal voltages, $v(t)$ and

internal states, $y(t)$). The set of equations (3.1) is consistent in the sense that the number of external states and the number of internal equations equals the number of external and internal equations respectively.

Note that equation (3.1) may contain linear and nonlinear terms. Equation (3.1) is quadratized; i.e., it is converted into a set of quadratic equations by introducing a series of intermediate variables and expressing the nonlinear components in terms of a series of quadratic terms. The resulting equations are integrated using a suitable numerical integration method. Assuming an integration time step h , the result of the integration is given with a second order equation of the form:

$$\begin{bmatrix} i(t) \\ 0 \end{bmatrix} = \begin{bmatrix} a_{11} & a_{12} \\ a_{21} & a_{22} \end{bmatrix} \begin{bmatrix} v(t) \\ y(t) \end{bmatrix} + \begin{bmatrix} (v^T(t), y^T(t))F_1 \begin{bmatrix} v(t) \\ y(t) \end{bmatrix} \\ (v^T(t), y^T(t))F_2 \begin{bmatrix} v(t) \\ y(t) \end{bmatrix} \\ \vdots \end{bmatrix} + \begin{bmatrix} b_1(t-h) \\ b_2(t-h) \end{bmatrix} \quad (3.2)$$

where: $i(t)$, $v(t)$, and $y(t)$ are the device terminal currents vector, external states vector and internal states vector respectively, and $b_1(t-h)$, $b_2(t-h)$ are past history functions.

Network Equations: The network solution is obtained by application of Kirchoff's current law at each node of the system. This procedure results in the set of equations (3.3). To these equations, the internal equations are appended resulting to the following set of equations:

$$\sum_k A^k i^k(t) = I_{inj} \quad (3.3)$$

$$\text{internal equations of all devices} \quad (3.4)$$

where I_{inj} is a vector of nodal current injections, A^k is a component incidence matrix with:

$$\begin{aligned} \{A_{ij}^k\} &= 1, \text{ if terminal } j \text{ of component } k \text{ is connected to node } i \\ &= 0, \text{ otherwise} \end{aligned}$$

$i^k(t)$ are the terminal currents of component k .

Note that Equations (3.3) correspond one-to-one with the external system states while Equations (3.4) correspond one-to-one with the internal system states.

The component k terminal voltage $v^k(t)$ is related to the nodal voltage vector $v(t)$ by:

$$v^k(t) = (A^k)^T v(t) \quad (3.5)$$

Solution of Network Equations: Upon substitution of device equations (3.2), the set of equations (3.3) and (3.4) become a set of quadratic equations:

$$Ax(t) + \begin{bmatrix} x^T(t)B_1(t)x(t) \\ x^T(t)B_2(t)x(t) \\ \vdots \end{bmatrix} + b(t-h) = 0 \quad (3.6)$$

where $x(t)$ is the vector of all external and internal system states.

These equations are solved using Newton's method. Specifically, the solution is given by the following expression.

$$x^{v+1}(t) = x^v(t) - J^{-1}(Ax^v(t) + \begin{bmatrix} x^{vT}(t)B_1(t)x^v(t) \\ x^{vT}(t)B_2(t)x^v(t) \\ \vdots \end{bmatrix} + b(t-h)) \quad (3.7)$$

where: J is the Jacobian matrix of equations (3.6) and $x^v(t)$ are the values of the state variables at the previous iteration.

3.2 Frequency Domain Analysis

Starting from the quadratized equations (3.1) and assuming that the device operates under steady state (single frequency) conditions, equations (3.1) are transformed into the following set of complex equations:

$$\begin{bmatrix} \tilde{I}^k \\ 0 \end{bmatrix} = y_{eq_cmpx}^k \begin{bmatrix} \tilde{V}^k \\ \tilde{Y}^k \end{bmatrix} + F \left\{ \begin{bmatrix} x^{kT} f_{eq_real1}^k x^k \\ x^{kT} f_{eq_real2}^k x^k \\ \vdots \end{bmatrix} \right\} - b_{eq_cmpx}^k \quad (3.8)$$

where \tilde{I}^k : vector of terminal currents
 \tilde{V}^k : vector of terminal voltages
 \tilde{Y}^k : vector of device internal state variables
 $\tilde{X}^k = \begin{bmatrix} \tilde{V}^k & \tilde{Y}^k \end{bmatrix}^T$

and $y_{eq_cmpx}^k$, $b_{eq_cmpx}^k$, and $f_{eq_real}^k$ are matrices with appropriate dimensions. x^k is obtained from the complex state \tilde{X}^k by replacing each element with its corresponding 2×1 vector that consists of the real part and the imaginary part. $F(\bullet)$ denotes a function mapping from a real vector to a complex vector. Note that this form includes two sets of equations, which are named *external*

equations and *internal equations* respectively. The terminal currents appear only in the external equations. Similarly, the device states consist of two sets: *external states* (i.e., terminal voltages, \tilde{V}^k) and *internal states*, \tilde{Y}^k . The set of equations (3.8) is consistent in the sense that the number of external states and the number of internal states equals the number of external and internal equations respectively. The form of equations (3.8) resembles the Norton form for electrical components. For this reason we have named the model expressed with Equation (3.8) the Generalized Norton Form (GNF).

Network Equations: The network equations are obtained by application of the connectivity constraints among components. For electrical circuits, the connectivity constraints are simply Kirchoff's current law at each node of the system. This procedure results in the set of equations (3.9). To these equations, the internal equations are appended resulting in the set of equations (3.9) and (3.10):

$$\sum_k A^k \tilde{I}^k = 0 \quad (3.9)$$

$$\text{internal equations of all devices} \quad (3.10)$$

where \tilde{I}^k is component k terminal currents composed of the currents at the composite nodes k_1, k_2, \dots, A^k is a component incidence matrix defined with:

$$\begin{aligned} \{A_{ij}^k\} &= 1, \text{ if terminal } j \text{ of component } k \text{ is connected to node } i \\ &= 0, \text{ otherwise} \end{aligned}$$

Let \tilde{V} be the vector of voltages at all the nodes of the system grouped by composite nodes. Then, the following relationship holds:

$$\tilde{V}^k = (A^k)^T \tilde{V} \quad (3.11)$$

where \tilde{V}^k is the vector of component k terminal voltages. Upon substitution of device equations (3.8) and incidence equations (3.11), the set of equations (3.9) and (3.10) become a set of quadratic equations:

$$\tilde{Y}\tilde{X} + F \begin{bmatrix} x^T f_1 x \\ x^T f_2 x \\ \vdots \end{bmatrix} - \tilde{B} = 0 \quad (3.12)$$

where \tilde{X} is the vector of states composed of all the components' state \tilde{X}^k ; x is the vector of network states composed of all the components' state x^k ; \tilde{Y} , f , and B are matrices with appropriate dimensions. These equations are the network equations. The simultaneous solution of these equations is obtained via Newton's method described next.

Solution of Network Equations: The numerical algorithm for solving the network equations (3.12) consists of two steps. First, we convert the network equations (3.12) into Cartesian

coordinates by simply replacing each complex variable with its Cartesian form and separating the real and imaginary parts of the complex equations. The procedure is equivalent with replacing each element in \tilde{Y} with its corresponding 2×2 Hermetian matrix. In particular, \tilde{Y}_{ij} is replaced by:

$$\tilde{Y}_{ij} \rightarrow \begin{bmatrix} \tilde{Y}_{ij}^r & -\tilde{Y}_{ij}^i \\ \tilde{Y}_{ij}^i & \tilde{Y}_{ij}^r \end{bmatrix}$$

where superscript r denotes real part and superscript i denotes imaginary part. Then, equation (3.12) is transformed into Equation (3.13) below:

$$Y_{real} x + \begin{bmatrix} x^T f_1 x \\ x^T f_2 x \\ \vdots \end{bmatrix} - B_{real} = 0 \quad (3.13)$$

Equation (3.13) is solved using Newton's method. Specifically, the solution is given by the following algorithm:

$$x^{v+1} = x^v - J^{-1} \left\{ Y_{real} x^v + \begin{bmatrix} x^{vT} f_1 x^v \\ x^{vT} f_2 x^v \\ \vdots \end{bmatrix} - B_{real} \right\} \quad (3.14)$$

where v is the iteration step number; J is the Jacobian matrix of equations (3.13). In particular, the Jacobian matrix takes the following form:

$$J = Y_{real} + \begin{bmatrix} x^{vT} (f_1 + f_1^T) \\ x^{vT} (f_2 + f_2^T) \\ \vdots \end{bmatrix}$$

Algorithm (3.14) guarantees quadratic convergence since it is Newton's method applied to a set of quadratic equations. In fact, algorithm (3.14) converges in two or three iterations.

3.3 Example Model: Generalized Conduit Enclosed Power Circuit

The model of a general conduit enclosed circuit is shown in Figure 3.1. There are two metallic conduits, each conduit encloses a circuit. The various conduits may be constructed from permeable material (magnetic) or nonmagnetic metallic or nonmetallic. The presented methodology addresses all possibilities. The model equations for this system are described next.

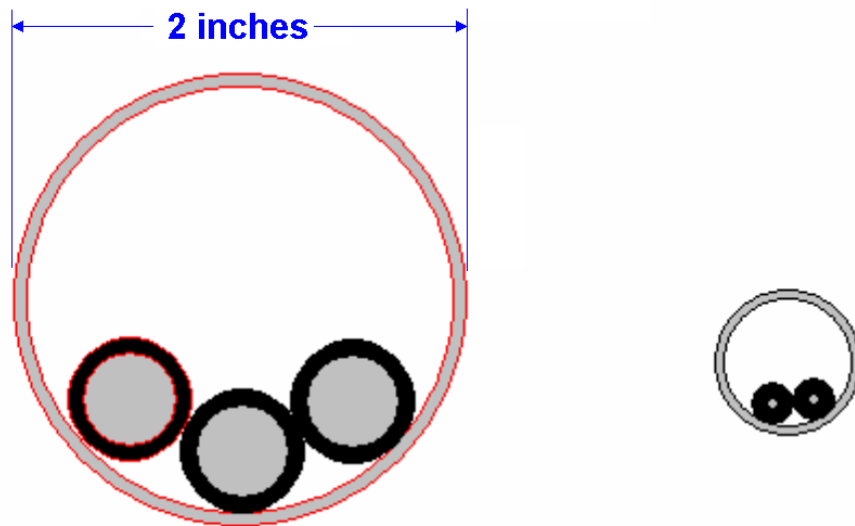


Figure 3.1. A General Conduit Enclosed Circuit

3.3.1 Modeling of General Conduit Enclosed Circuit – Magnetic Conduit

A general model of conduit enclosed circuits has been developed. The conduit may be metallic permeable (magnetic) or non-permeable (non-magnetic) material. This section describes the model when the conduit is permeable (magnetic).

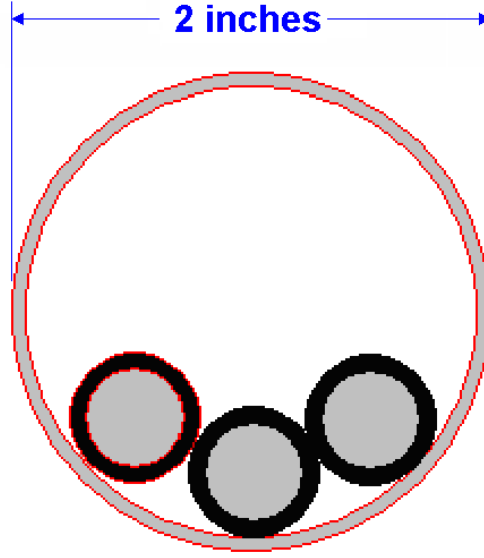


Figure 3.2. A Magnetic Conduit Enclosed Circuit

The geometry of this problem is shown in Figure 3.2. The magnetic properties of the conduit are described through the magnetic field dependent relative permeability $\mu_r(H)$ given by

$$\mu_r(H) = \begin{cases} \mu_{r,\max}, & H \leq \frac{B_s}{\mu_0 \mu_{r,\max}} \\ 1.0 + \mu_{r,\max} \left(1 - \frac{1}{\mu_{r,\max}} \right) \left(\frac{B_s}{\mu_0 \mu_{r,\max} H} \right)^\alpha, & H > \frac{B_s}{\mu_0 \mu_{r,\max}} \end{cases} \quad (3.15a)$$

$$\mu_r(H) = 1.0 \quad (3.15b)$$

where H is the total magnetic field intensity in the magnetic material, μ_0 is the free space permeability, and B_0 , H_0 , α , and $\mu_{r,\max}$ are material dependent parameters.

Equation (3.15a) applies to magnetic conduit and equation (3.15b) applies to the remaining part of the system (i.e., the power conductors, the insulation and the air).

Typical values for the constants appearing in above equations are:

$$B_s = 0.5 \text{ Tesla}, \quad \mu_{r,\max} = 1,300.0, \quad \text{and} \quad \alpha = 8.$$

The plot of relative permeability versus magnetic field intensity for the above parameters is illustrated in Figure 3.3.

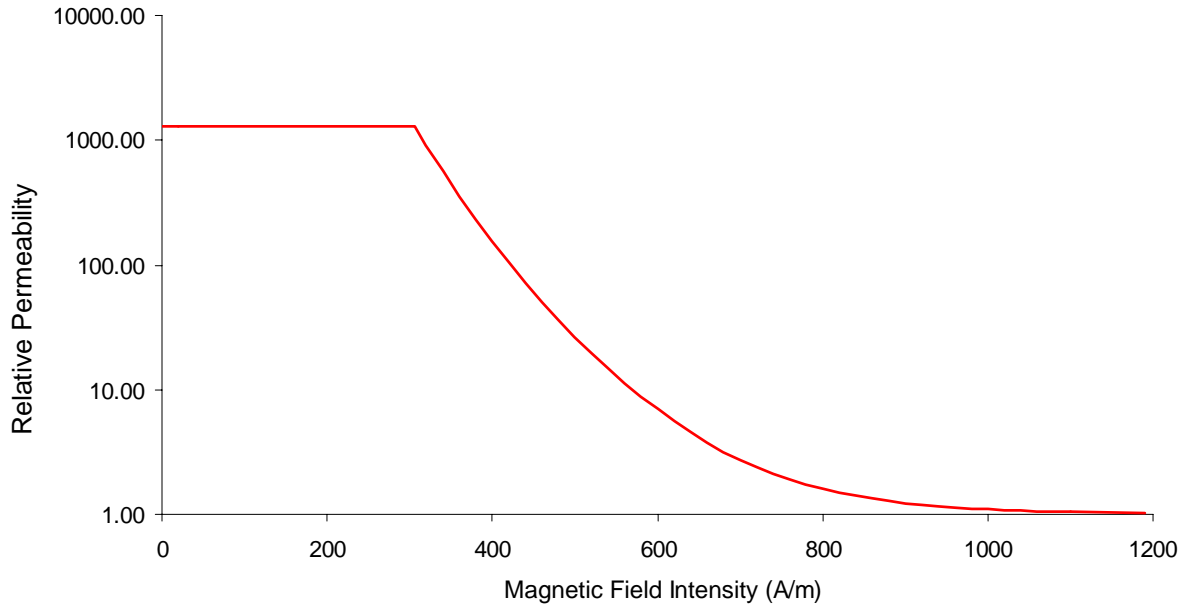


Figure 3.3. Relative Permeability versus Magnetic Field Intensity

The magnetic field analysis problem is inherently nonlinear due to the presence of the permeable material (magnetic) conduit. In modeling this system, a quasi-static (for low frequencies as well as the 60 Hz of the power system) approach has been employed [2]. The magnetic field \vec{H} (vector variable) in every region is written as a sum of two terms:

$$\vec{H} = \vec{H}_c + \vec{H}_m \quad (3.16)$$

where the first term, \vec{H}_c , is the magnetic field that results from assuming that everything in the system remains identical to the original problem except that the conduit material is non-magnetic (non-permeable). The second term, \vec{H}_m , expresses the perturbation of the magnetic field due to the presence of the magnetic material in the conduit region. Using this approach, the original problem is broken down into two sub-problems. The first sub-problem involves the solution of the magnetic field problem in the case of a system of non-magnetic conductors and conduit. The first sub-problem is solved with standard techniques described in many textbooks including [3].

The term \vec{H}_c satisfies the following Maxwell's equation:

$$\nabla \times \vec{H}_c = \vec{J} \quad (3.17)$$

where the radiation term (displacement current has been dropped due to the quasi-static approximation). The term \vec{J} denotes the current density which is determined from the solution of the first sub-problem along with the calculation of \vec{H}_c . Since the total magnetic field \vec{H} also satisfies Equation (3.17) it can be deduced that \vec{H}_m satisfies the homogeneous curl equation $\nabla \times \vec{H}_m = 0$ and consequently it can be expressed as the gradient of a scalar magnetic potential function Φ :

$$\vec{H}_m = -\nabla\Phi \quad (3.18)$$

It follows that the divergence of the total magnetic potential Φ satisfies the following equation:

$$\nabla \cdot (\mu \nabla \Phi) = \nabla \cdot (\mu \vec{H}_c) \quad (3.19)$$

In above equation \vec{H}_c is known from the solution of the first sub-problem (the non-magnetic material sub-problem). For a region of constant relative permeability the above equation is written in the form

$$\mu \nabla^2 \Phi = \mu \nabla \cdot \vec{H}_c = 0 \quad (3.20)$$

since the \vec{H}_c magnetic field has also a zero divergence. The last equation is a Laplace equation for the scalar magnetic potential Φ . Equation (3.20) needs to be solved for each region of the second sub-problem which is depicted in Figure 3.2. Since there is a magnetic material (steel conduit), the scalar magnetic potential must satisfy a boundary condition at the boundaries between materials of differing relative permeability ($r = a_{in}$, and $r = a_{out}$ in Figure 3.4). At these boundaries the normal component of the total magnetic flux density must be continuous. If $r = r_b$ represents the boundary surface between two media of permeabilities μ_1 and μ_2 , then the following conditions must be satisfied:

$$\Phi_1(r = r_b) = \Phi_2(r = r_b) \quad (3.21)$$

$$\mu_1 H_{r1}(r = r_b) = \mu_2 H_{r2}(r = r_b)$$

or

$$\mu_1 \left[H_{cr1} - \frac{\partial \Phi_1}{\partial r} \right]_{r=r_b} = \mu_2 \left[H_{cr2} - \frac{\partial \Phi_2}{\partial r} \right]_{r=r_b} \quad (3.22)$$

where H_{ri}, H_{cri}, Φ_i , $i = 1, 2$ are the radial component of the total magnetic field, the radial component of \vec{H}_c (first sub-problem), and the scalar magnetic potential, respectively. However, the solution of the first sub-problem \vec{H}_c must satisfy the condition $H_{r1}(r = r_b) = H_{r2}(r = r_b) = H_{cr}(r = r_b)$ (continuity of normal H_c component). Using the last equality the second boundary condition is written as

$$\mu_1 \frac{\partial \Phi_1}{\partial r} \bigg|_{r=r_b} = \mu_2 \frac{\partial \Phi_2}{\partial r} \bigg|_{r=r_b} - (\mu_2 - \mu_1) H_{cr}(r=r_b) \quad (3.23)$$

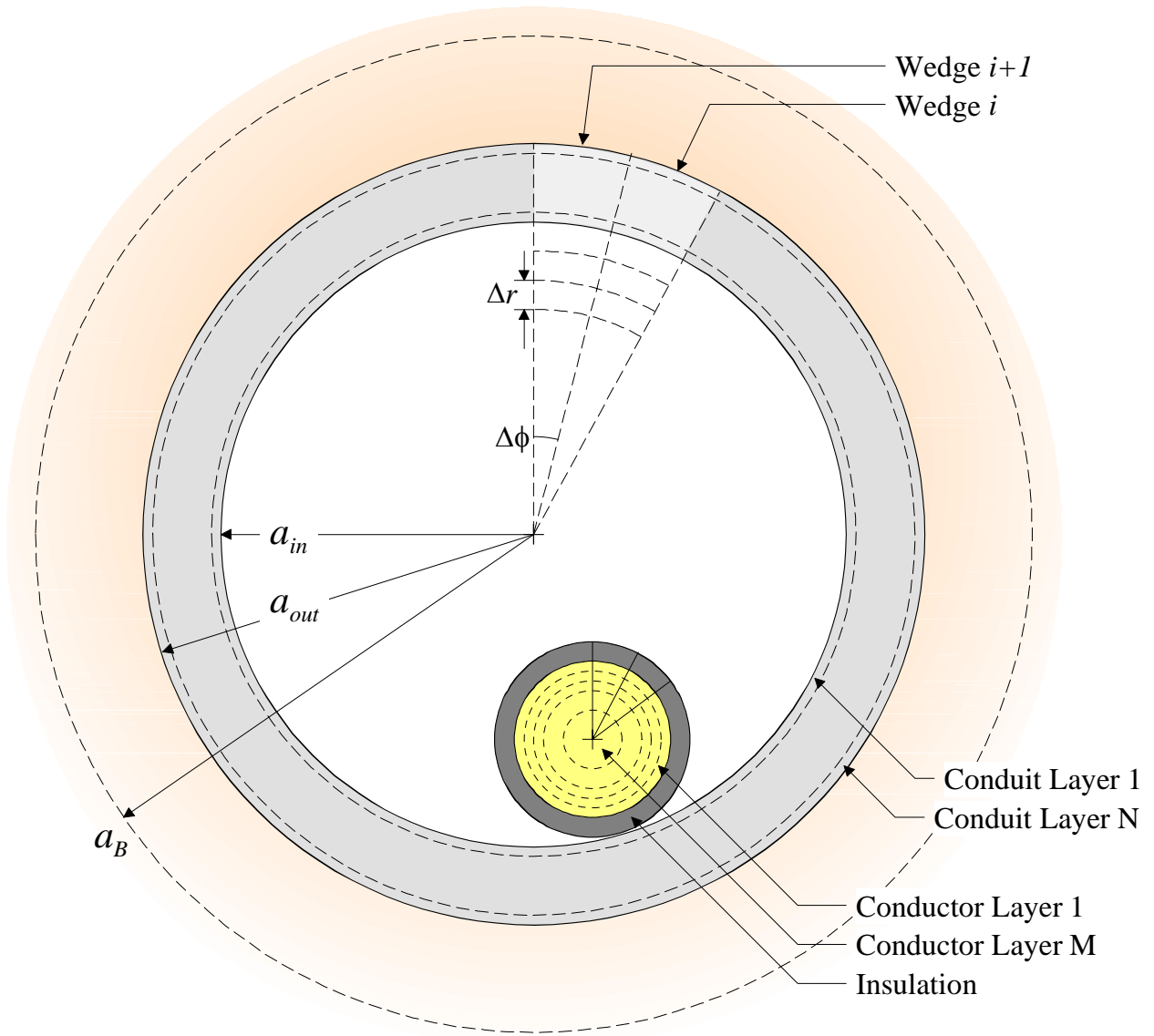


Figure 3.4. Illustration of Conduit Segmentation into Slices

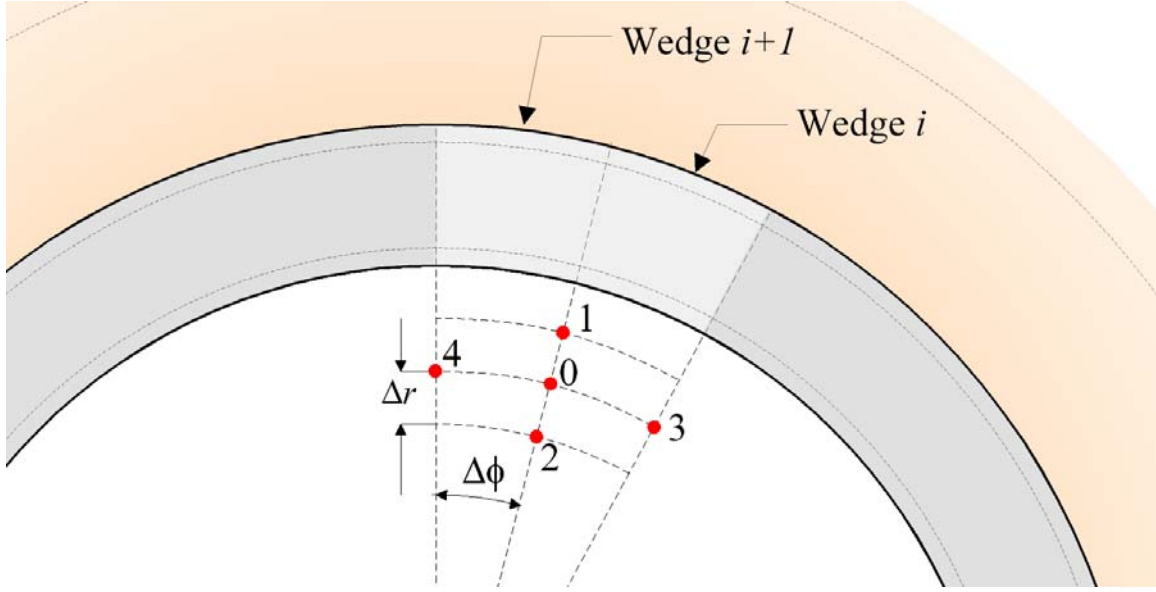


Figure 3.5. Detail of Segmentation and Notation for Difference Equations

The last equation contains the term $H_{cr}(r = r_b)$ which in general will have angular dependence since the non-magnetic conductors are eccentric. This term forces the scalar magnetic potential to also be an angular dependent quantity. Therefore for any region in which Equation (3.20) needs to be solved the scalar magnetic potential will have both radial and angular dependence; i.e., $\Phi = \Phi(r, \phi)$ (assuming a cylindrical coordinate system) and Equation (3.20) reduces to

$$\frac{\partial^2 \Phi}{\partial r^2} + \frac{1}{r} \frac{\partial \Phi}{\partial r} + \frac{1}{r^2} \frac{\partial^2 \Phi}{\partial \phi^2} = 0 \quad (3.24)$$

The resulting magnetic field \vec{H}_m is given by

$$\vec{H}_m = -\frac{\partial \Phi}{\partial r} \hat{r} - \frac{1}{r} \frac{\partial \Phi}{\partial \phi} \hat{\phi} \quad (3.25)$$

where \hat{r} and $\hat{\phi}$ are the unit radial and tangential vectors at point (r, ϕ) . Equations (3.24) and (3.25) cannot be solved analytically due to the angular and radial dependence of the scalar magnetic potential. These equations are solved using the finite-difference technique. The discretized equations and their corresponding boundary conditions are summarized in the next section.

Equation (3.24) also needs to be solved in the region outside the conduit. This region is unbounded. Since Equation (3.24) is solved numerically, an artificial boundary is used sufficiently far from the conduit at a distance $r = a_B$ (see Figure 3.4). At this artificial boundary a suitable boundary condition is used. There are two possible choices. The first one is to set the scalar magnetic potential at $r = a_B$ to zero since this potential tends to zero as $a_B \rightarrow \infty$. The second condition is to set the radial (normal) derivative of the magnetic scalar potential to zero. This is justified since at a sufficiently large distance away from the conduit-and-conductors system, the magnetic field will have a tangential component only. The latter is the boundary condition used in this analysis.

The above analysis is applied to all segments of the conduit (the segmentation of the conduit is illustrated in Figures 3.4 and 3.5). Specifically, the conduit is divided into a number (N in Figure 3.4) of concentric layers (rings) and the relative permeability of each layer is known and assumed to be constant within the layer. Then, Equation (3.24) is solved within each region under the boundary conditions described by Equations (3.21) and (3.22). After the calculation of the scalar magnetic potential the total magnetic field is computed everywhere. Consequently, a new estimate of the relative permeability profile of the conduit is computed. Then the procedure is repeated until the relative permeability profile of the conduit and the resulting total magnetic field are self-consistent; i.e., they satisfy Maxwell's equations.

In summary, the algorithmic steps of the solution are:

1. Calculation of the magnetic field \vec{H}_c that results from the solution of the non-magnetic problem (first sub-problem, Figure 3.4).
2. Separation of the conduit in N concentric layers with relative permeabilities specified from Equation (1) where $H = |\vec{H}_c|$.
3. Solution of the Laplace Equation (3.24) for each region of the second sub-problem (Figure 3.4) under the boundary conditions (3.21) and (3.22).
4. Calculation of the perturbation magnetic field \vec{H}_m from Equation (3.18).
5. Calculation of the total magnetic field from Equation (3.16).
6. Repetition of step 2 with relative permeabilities computed using the total magnetic field computed in step 5.
7. Repetition of step 2 through 6 until a self-consistent magnetic field profile and relative permeability profile are obtained.

The above described procedure is implemented using finite differences. The equations for the finite differences are given next.

3.3.2 Finite Difference Implementation

The Laplace's equation for the scalar magnetic potential Φ [Equation (3.24)] is discretized using a cylindrical two-dimensional grid as shown in Figure 3.4 and 3.5. It is assumed that within a region in which the Laplace's equation is solved the radial, Δr , and angular, $\Delta\phi$, grid spacings are constant. Considering the points 0 through 4 in Figure 3.5 we derive the difference equation corresponding to Equation (3.24):

$$\frac{\Phi_1 - 2\Phi_0 + \Phi_2}{(\Delta r)^2} + \frac{1}{r_0} \frac{\Phi_1 - \Phi_2}{2\Delta r} + \frac{\Phi_3 - 2\Phi_0 + \Phi_4}{(r_0\Delta\phi)^2} = 0 \quad (3.26)$$

which is also written as

$$2[1 + (\frac{\Delta r}{r_0\Delta\phi})^2]\Phi_0 = [1 + \frac{\Delta r}{2r_0}]\Phi_1 + [1 - \frac{\Delta r}{2r_0}]\Phi_2 + (\frac{\Delta r}{r_0\Delta\phi})^2\Phi_3 + (\frac{\Delta r}{r_0\Delta\phi})^2\Phi_4 \quad (3.27)$$

Φ_i ($i = 0, 1, \dots, 4$) is the scalar potential at grid points 0 through 4 respectively and r_0 is the radial coordinate of point 0. Equations (3.26) or (3.27) are written for any point within a homogeneous region in the grid.

Of particular interest are the points that lie at the boundary between two regions of differing permeability. In this case the boundary condition expressed by Equation (3.21) is written in a discretized form. The continuity of the scalar potential across a boundary is accomplished by using grid points exactly at the boundary surface between the different regions. In order to achieve the latter it is imperative to use unequal radial grid spacing from region to region. Assuming that S is the boundary between two regions 1 and 2 of permeabilities μ_1 and μ_2 (as shown in Figure 3.5) the radial grid spacings are Δr_1 and Δr_2 respectively. It is noted that it is not necessary to have unequal angular grid spacing for this problem. With a lengthy derivation (not included here) the discretized form of Equation (3.21) is given by the following expression:

$$\left[2 \frac{\Delta r_2}{\Delta r_1} \frac{\mu_1(1 - \frac{\Delta r_2}{2r_0}) + \mu_2(1 + \frac{\Delta r_1}{2r_0}) \frac{\Delta r_1}{\Delta r_2}}{\mu_1(1 - \frac{\Delta r_2}{2r_0}) + \mu_2(1 + \frac{\Delta r_1}{2r_0}) \frac{\Delta r_2}{\Delta r_1}} + 2 \frac{\Delta r_1 \Delta r_2}{r_0^2 \Delta\phi^2} \right] \Phi_0 =$$

$$\frac{2\mu_2(1 + \frac{\Delta r_1}{2r_0})}{\mu_1(1 - \frac{\Delta r_2}{2r_0}) + \mu_2(1 + \frac{\Delta r_1}{2r_0}) \frac{\Delta r_2}{\Delta r_1}} \Phi_1 + \frac{2\mu_1(1 - \frac{\Delta r_2}{2r_0})}{\mu_1(1 - \frac{\Delta r_2}{2r_0}) + \mu_2(1 + \frac{\Delta r_1}{2r_0}) \frac{\Delta r_2}{\Delta r_1}} \Phi_2 + \quad (3.28)$$

$$\frac{\Delta r_1 \Delta r_2}{r_0^2 \Delta\phi^2} (\Phi_3 + \Phi_4) - \frac{\Delta r_2}{2} \frac{4(\mu_2 - \mu_1)(1 + \frac{\Delta r_1}{2r_0})(1 - \frac{\Delta r_2}{2r_0})}{\mu_1(1 - \frac{\Delta r_2}{2r_0}) + \mu_2(1 + \frac{\Delta r_1}{2r_0}) \frac{\Delta r_2}{\Delta r_1}} H_{cr0}$$

Note that equation (3.28) reduces to Equation (3.26) in the case of a homogeneous region when $\mu_1 = \mu_2$ and $\Delta r_1 = \Delta r_2 = \Delta r$.

The outer artificial boundary at $r = a_B$ needs to be treated as follows. The points on this boundary satisfy the condition $\frac{\partial \Phi}{\partial r} = 0$. A lengthy derivation (not shown here) leads to the conclusion that each point in the artificial boundary satisfies the following discretized boundary condition:

$$(2 + 2 \frac{\Delta r^2}{r_0^2 \Delta \phi^2}) \Phi_0 = 2\Phi_2 + \frac{\Delta r^2}{r_0^2 \Delta \phi^2} (\Phi_3 + \Phi_4) \quad (3.29)$$

Finally, the origin of cylindrical coordinate system satisfies the condition

$$\Phi_0 = \frac{1}{N} \sum_{i=1}^N \Phi_i \quad (3.30)$$

where Φ_i ($i = 1, 2, \dots, N$) are the closest neighbor to the origin points.

Equations (3.27) or (3.28) or (3.29) or (3.30) are written for each grid point of the problem defined in Figure 3.4 and 3.5 (second sub problem). These equations form a set of linear equations which can be written in the following compact matrix notation.

$$[A][\Phi] = [b] \quad (3.31)$$

where $[A]$ is a coefficient matrix of dimensions $m \times m$ (where m is the total number of grid points), $[\Phi]$ is a vector of length m containing the scalar magnetic potential of the grid points, and $[b]$ is the source vector of length m the nonzero terms of which are due to the boundary condition (3.22).

The solution of the system of equations (3.31) specifies the scalar magnetic potential at each grid point. Then, the \vec{H}_m can be found using the discretized form of equation (3.18). The discretization procedure of equation (3.18) is lengthy but straightforward procedure yielding:

$$\begin{aligned} \vec{H}_m \Big|_0 = & - \frac{\partial \Phi}{\partial r} \Big|_0 \hat{r}_0 - \frac{\partial \Phi}{\partial \phi} \Big|_0 \hat{\phi}_0 - \frac{\Phi_4 - \Phi_3}{2\Delta \phi} \hat{\phi}_0 - \\ & \left(\frac{2}{\Delta r} + \frac{1}{r_0} \right)^{-1} \left[\frac{2}{\Delta r^2} (\Phi_0 - \Phi_2) - \frac{1}{r_0^2 \Delta \phi^2} (\Phi_3 + \Phi_4 - 2\Phi_0) \right] \hat{r}_0 \end{aligned} \quad (3.32)$$

where $\hat{r}_0 = \hat{x} \cos \phi_0 + \hat{y} \sin \phi_0$ and $\hat{\phi}_0 = -\hat{x} \sin \phi_0 + \hat{y} \cos \phi_0$ (hatted variables denote unit vectors).

4.0 Power Quality Assessment

The quality of power at the consumer site is affected by (a) temporary disturbances that may originate anywhere in the system and (b) waveform distortion from nonlinear loads. The sources of disturbances are multiple and with varying parameters. For example, in many places of the world, the most frequent disturbances originate from lightning activity near electric installations. Lightning generates overvoltages that may result in flashover causing voltage sags to some portion of the distribution system, voltage swell to other areas, as well as interruption of power. The number of customers affected depends on the design of the system and placement of interruption devices, while the level of voltage sags or swells may depend on the grounding system, size of neutral, etc. Thus, the grounding system design plays an important role on the performance of the system from the PQ point of view. The modeling and analysis methodology presented in the previous section is well suited for this application. It is also pointed out that many of the causes are statistically distributed both in time and in space. Statistical methods represent the best way for meaningful assessment of their effects on power quality.

In this section we first present the application of the proposed methodologies on specific power quality problems. Subsequently, we apply statistical methods using the physically based models of the system to provide an excellent tool for correlating design options to power quality performance. For example, we consider a typical distribution system consisting of a typical overhead distribution system, underground feeders, electric loads, motors, and other types of nonlinear loads. This system may be subjected to a number of disturbances, exogenous such as lightning as well as system internal disturbances such as motor start-up and shutdown, distorting loads, switchings, and power electronic based controllers. Depending on the phenomena to be studied, specific devices and or events are imposed on the system. In this section we present specific examples of the types of analyses necessary. Then, we connect all these analyses with a Monte Carlo Simulation for the purpose of statistically assessing the power quality performance of a system. This approach is very useful for meaningful and cost effective improvements of the system to maximize power quality.

4.1 Harmonics

Harmonic generation and propagation can be studied with the proposed methodology by connecting various types of distorting loads and examining the harmonic content of voltages or currents anywhere in the system. Specifically, a harmonic analysis on any voltage or current anywhere in the system can be performed. As an example, Figure 4.1 illustrates a harmonic analysis of the Phase A current on the high side of the transformer for a specific operating condition. This figure is obtained by capturing one cycle of the solution of the system at a specific node (voltage) or terminal (current) of the system and subsequent Fourier analysis of the waveform.

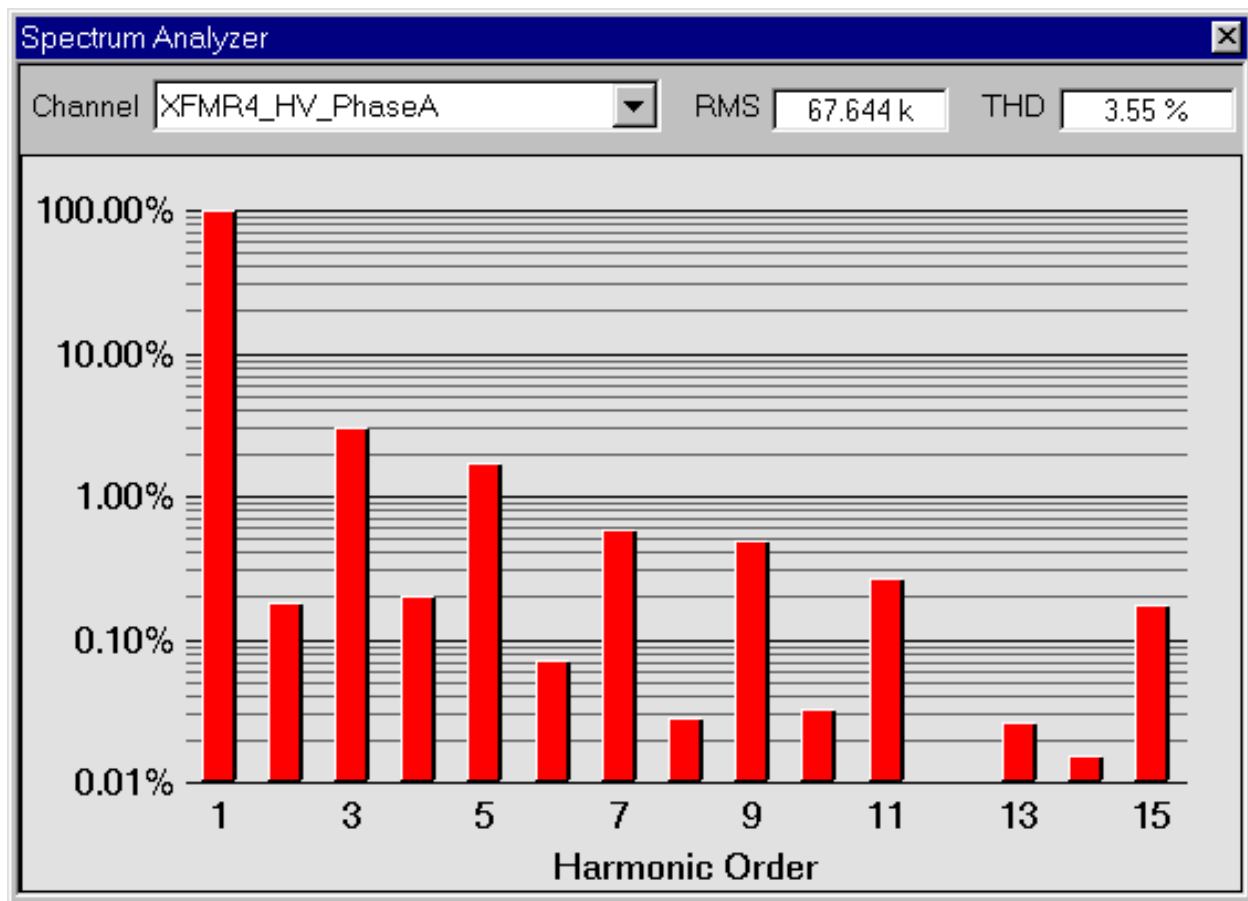


Figure 4.1. Spectrum Analyzer Display of a Specific Voltage Waveform

Another more important issue associated with harmonics is the issue of harmonic resonance. For this purpose the described analysis method is performed for an appropriate set of frequencies. At each frequency the impedance or transimpedance of the system is computed and presented in the form of a graph (frequency scan or Bode plot). As an example, Figures 4.2, 4.3 and 4.4 present the results of this analysis. Figure 4.2 illustrates the example system. Note that it is a small section of a typical distribution circuit with voltage correction capacitors placed at specific points of the system. Note also that the grounding of the system is modeled. Figure 4.3 illustrates the positive sequence impedance as a function of frequency at BUS70 of the system, while Figure 4.4 illustrates the impedance between phase A and neutral at the same BUS70 of the system as a function of frequency. It is pointed out that the resonance characteristics of Figure 4.3 are mainly affected by the positive sequence impedance of the system. In this case the design of the grounding system has very little or no effect on the resulting resonance characteristics. On the other hand, the data of Figure 4.4 are affected by the size of the neutral wire of the system, the groundings of the distribution line and the soil resistivity. In terms of familiar nomenclature, we state that the results of Figure 4.4 depend on positive, negative and zero sequence impedances of the system and the zero sequence impedance is affected by the grounding system design (it is pointed out that the analysis method does not use the positive, negative and zero sequence impedances for modeling the circuit but rather the physically based model of the distribution circuit). This means that grounding does affect the resonance characteristics of the system for the condition of Figure 4.3 (positive sequence). Comparing the two figures (4.3 and 4.4) it is

apparent that there is a common resonance frequency at 334 Hz. The resonance Q is quite high for the positive sequence resonance ($Z=872$ ohms) and much lower for the phase to neutral resonance ($Z=163$ ohms). This result should be expected since the grounding system does introduce a substantial resistive component in the phase A to neutral impedance of the circuit. This component can be controlled by appropriate grounding system design procedures. Note that the grounding resistance is beneficial in reducing the resonance Q.

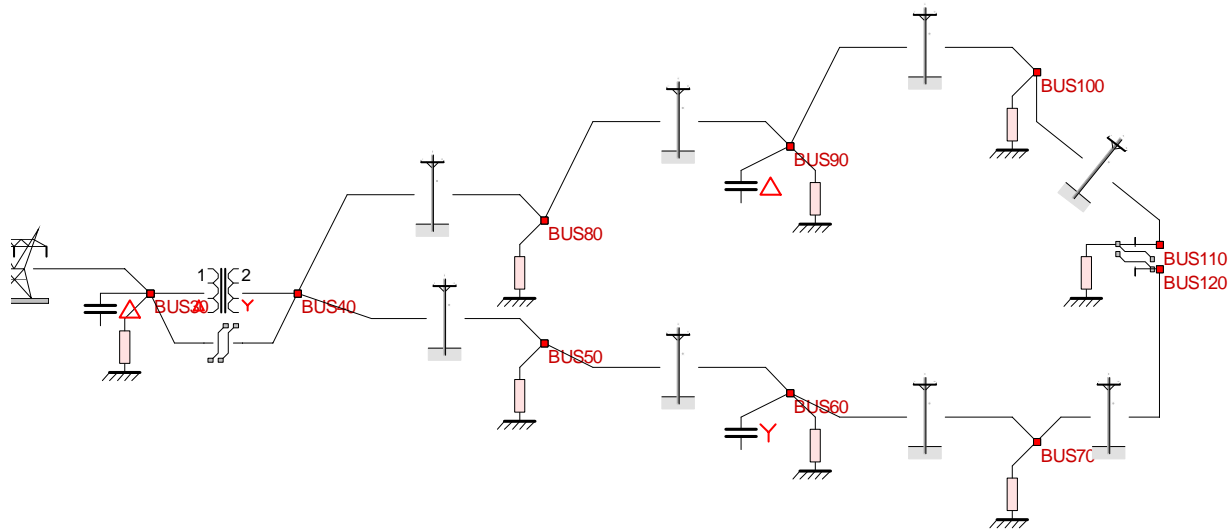


Figure 4.2. Example Test System for Harmonic Resonance

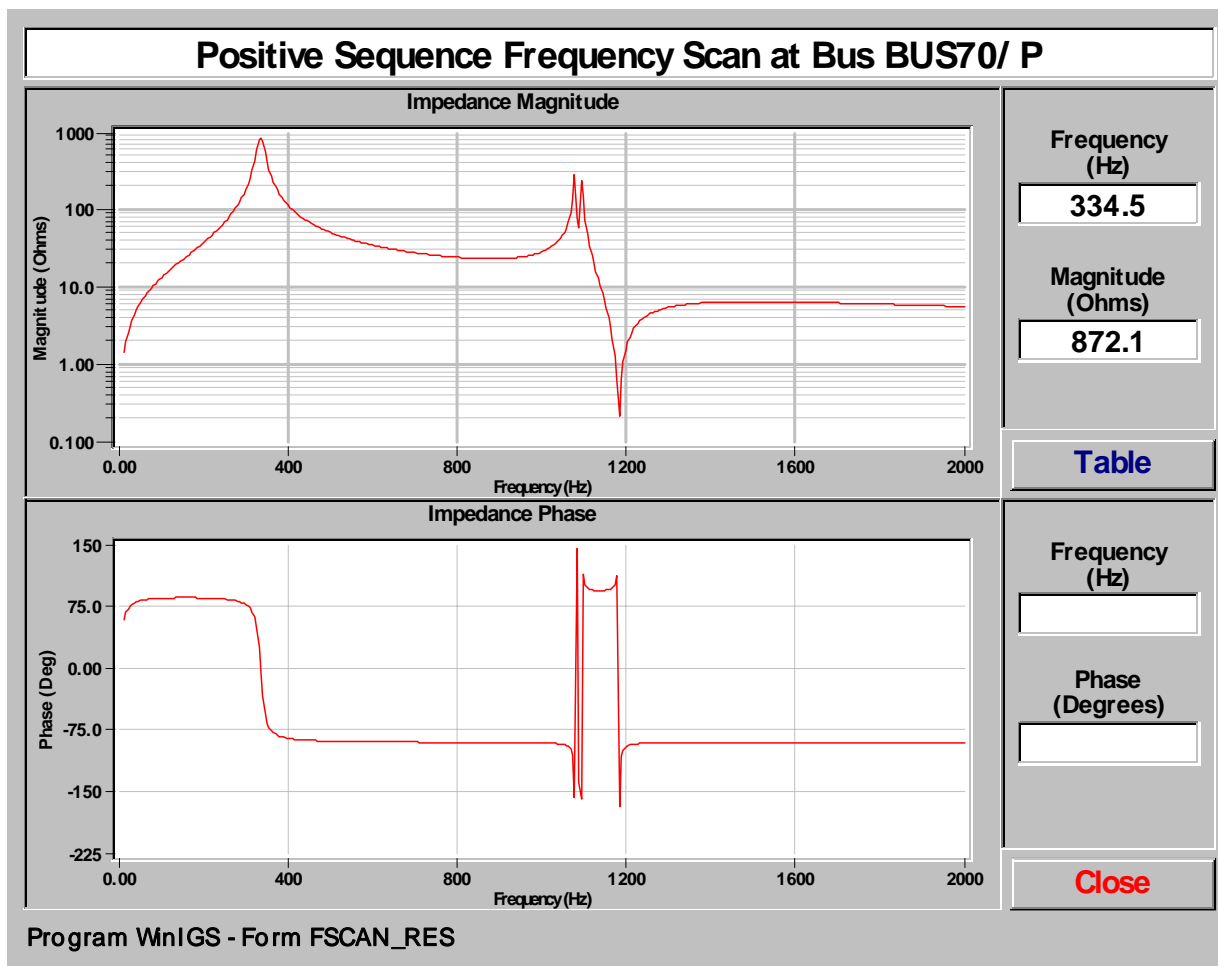


Figure 4.3. Positive Sequence Harmonic Resonance – BUS70

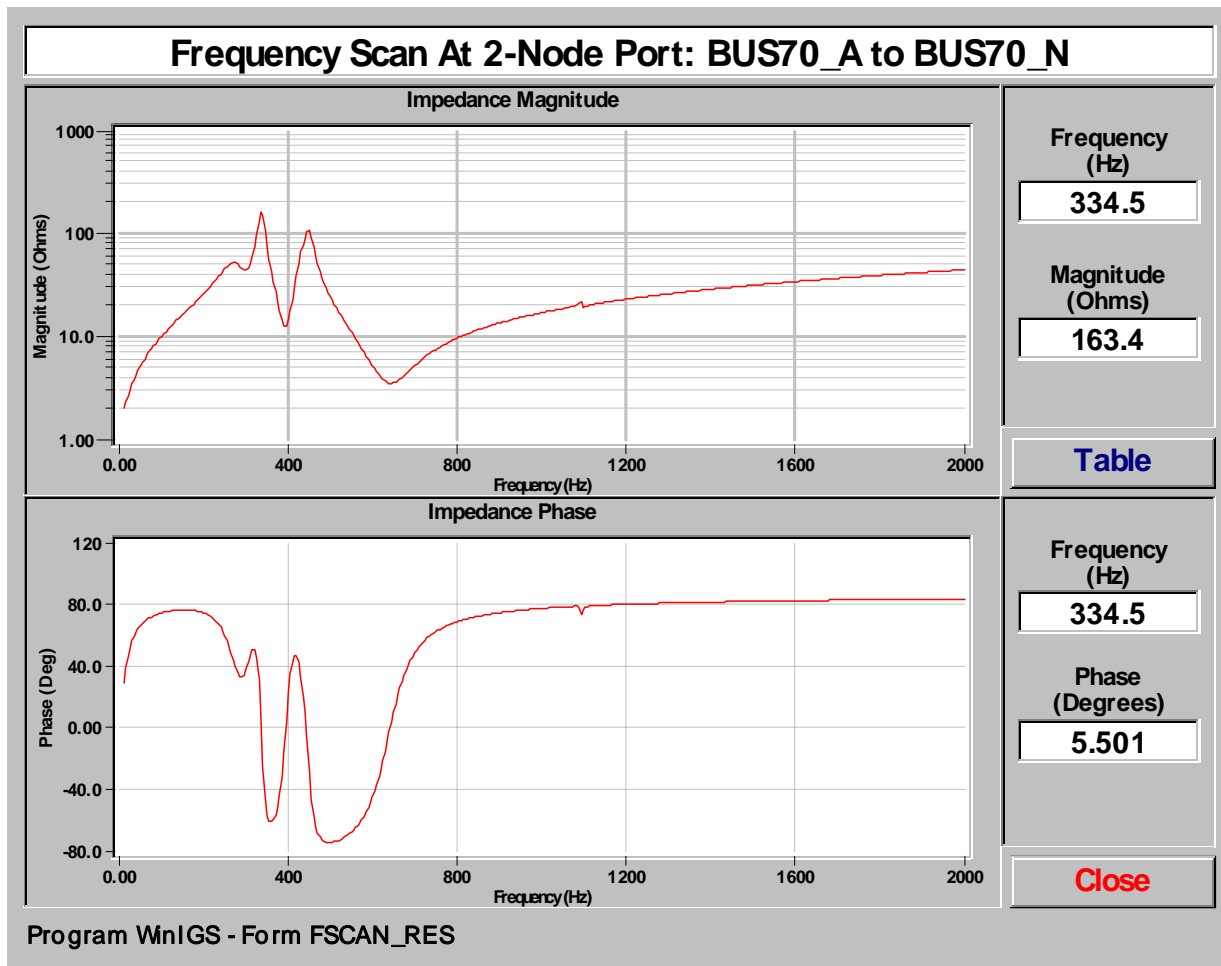


Figure 4.4. Phase A to Neutral Resonance at BUS70

It is important to note that this tool provides the capability to quantitatively study the effects of alternate grounding system designs on resonance frequencies and resonance Q. This capability is demonstrated with the system of Figure 4.5. The system consists of a typical distribution circuit that feeds a six pulse converter load. The major parameters of the system are listed in the figure. The driving impedance graph at the point of common coupling with the six pulse converter load is given in Figures 4.6 and 4.7 for the positive sequence and zero sequence respectively. The impact of alternative grounding arrangements on the resonance Q has been studied with this example. The resonance performance of the positive sequence is not sensitive to grounding arrangements. However the resonance performance of the zero sequence is very sensitive. As an example, Table 4.1 provides the resonance Q for the system of Figure 4.5 as a function of the grounding impedance of the capacitor banks, BUS1 and BUS2. Note that as the grounding resistor is increasing, the resonance Q is decreased.

Table 4.1 Resonance Q versus Grounding Impedance

R-Ohm	0	1	2	4	10
Q	9.41	7.07	5.73	4.21	2.77

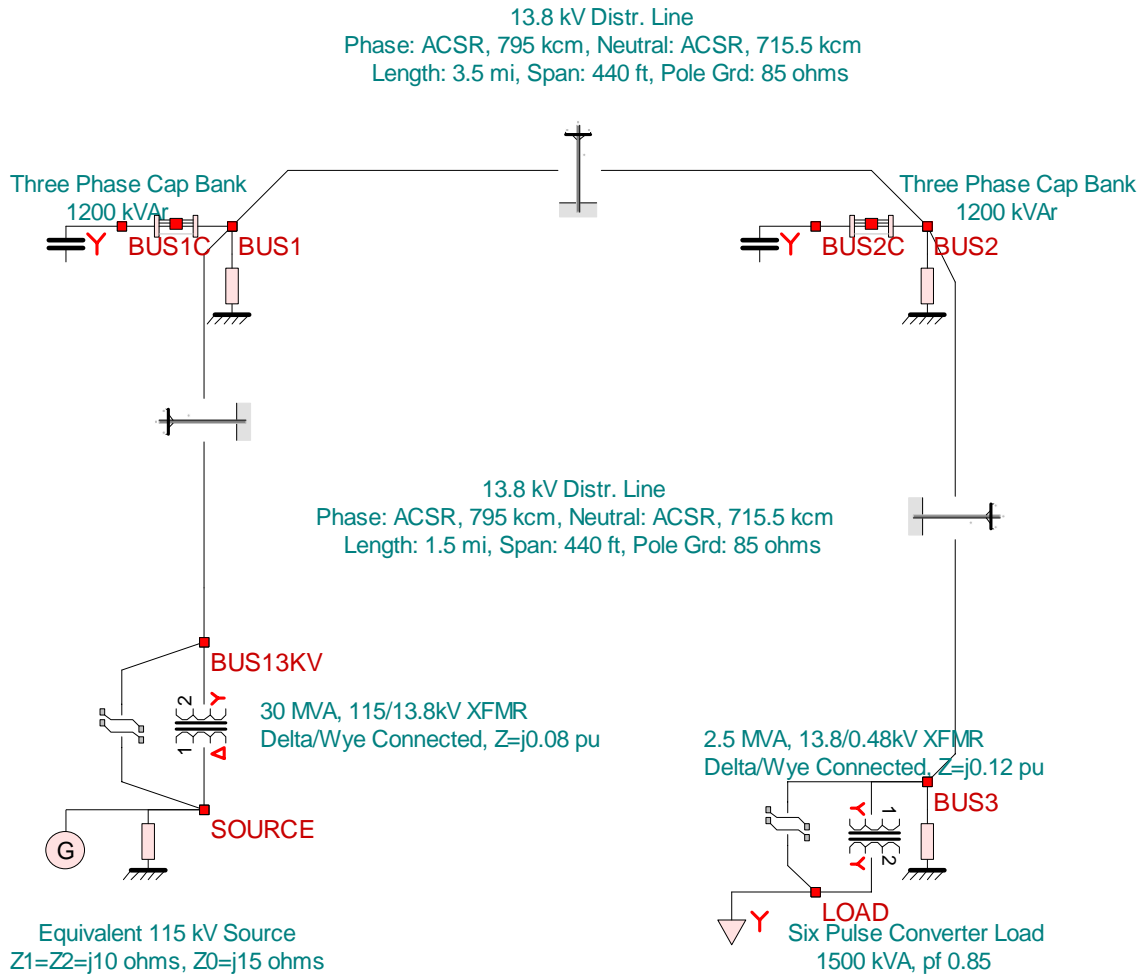


Figure 4.5. Example Test System for Harmonic Resonance

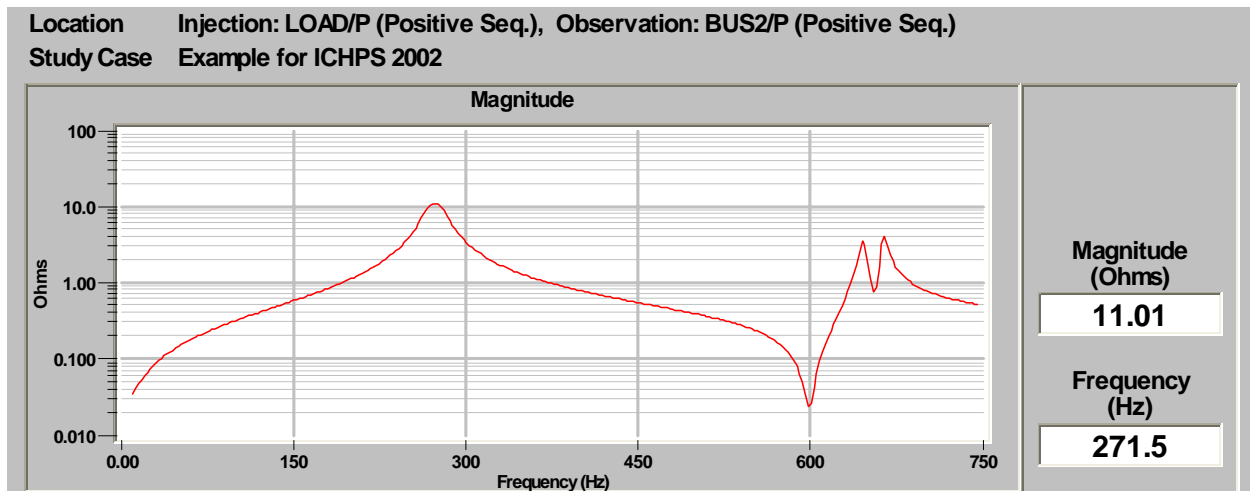


Figure 4.6. Positive Sequence Trans-Impedance (LOAD to BUS2)

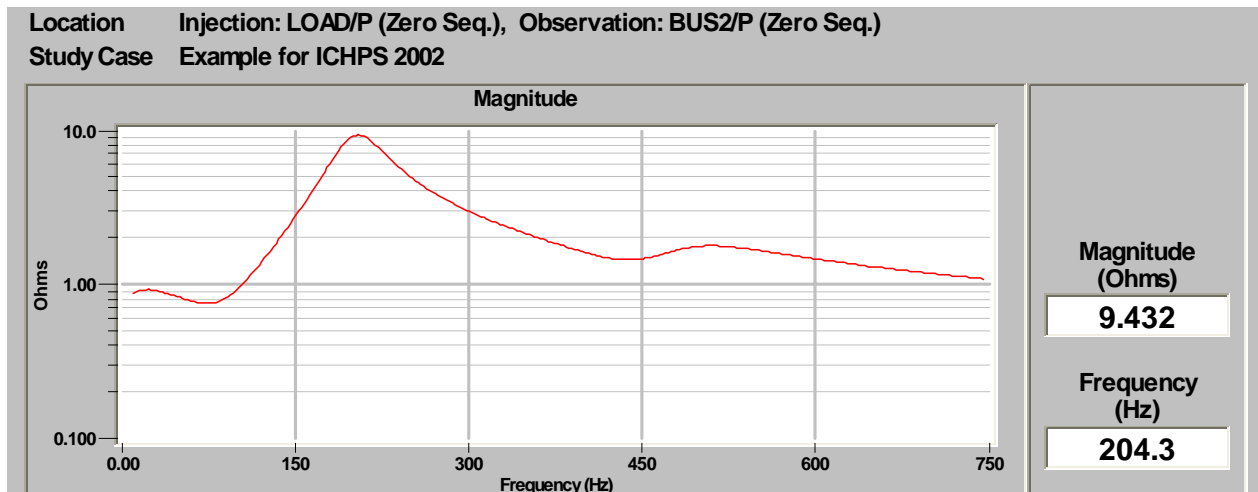


Figure 4.7. Zero Sequence Trans-Impedance (LOAD to BUS2)

4.2 Electromagnetic Fields

Another major issue is the electromagnetic (EM) field generated by power circuits. These fields have three major effects. The first is the much debated issue of biological effects of electromagnetic fields. Specifically, EM fields may be hazardous to health. Numerous studies have been produced, some of them affirming the biological effects, some showing a relatively small statistical biological effect. IEEE has adopted the policy of “prudent avoidance” of excessive electromagnetic fields. In this research project our focus is to develop methodologies for accurate computation of electromagnetic fields for any design of the system and in particular

any design of grounding systems. The second effect is the phenomenon of interaction with sensitive electronic devices, such as TVs, computer monitors, PLCs, etc. The third effect is the impact of electromagnetic fields on the distribution of electric currents in power circuits. Specifically, electromagnetic fields interact with the current flow in conductors causing uneven distribution of current within a conductor or uneven split of currents in multiple conductors that are connected in parallel. This phenomenon is particularly prominent in multiple parallel circuits. Uneven current distribution may cause circuit overheating and insulation failures. To avoid these problems these phenomena must be taken into account in the design of power distribution circuits. One approach to account for uneven current distribution effects is to specify circuit conductor sizes using **derated** conductor ampacities. The derating factors are computed by analyzing the current distributions for the specific circuit topology. The proposed methodology is particularly suitable for these computations. Reference [9] describes the overall approach using the methodology developed in the program GEMI (see also Appendix A).

4.3 Voltage Sags and Swells

Sequences of fault initiation, fault clearing and reclosing can be studied with the proposed methodology by simply inserting a fault, waiting for the breaker logic to interrupt the circuit and then reclose. For a single phase to ground fault, voltage sags can be observed at some loads and voltage swells can be observed at other loads. The level of voltage sags and swells is dependent upon the design of the system and the impedances of the system.

Voltage Sags and Swells: Sequences of fault initiation, fault clearing and reclosing result in voltage sags for certain customers and voltage swells for others. The level of the voltage swells and sags depends on grounding system design. This fact had been recognized long time ago. For example, an IEEE committee has drafted the nomogram of Figure 4.8. The data of Figure 4.8 have been computed with an approximate model based on sequence parameters representation of the power system. This nomogram provides the percent voltage (voltage swell) on the unfaulted phases for a single line to ground fault at the same location as a function of the zero sequence resistance (R_0), zero sequence reactance (X_0) and positive sequence reactance (X_1). Note that the zero sequence components depend on the design of the grounding system and the voltage swells depend on the zero sequence impedance. The method presented in this paper provides the exact voltage swells and voltage sags for any fault at any location and for any design system in terms of neutral size, grounding design, etc. As an example, Figure 4.9 illustrates the voltage swells and sags along a circuit during a single line to ground fault. Note that the two unfaulted phases experience a different level of voltage sags and swells due to the asymmetry of the system.

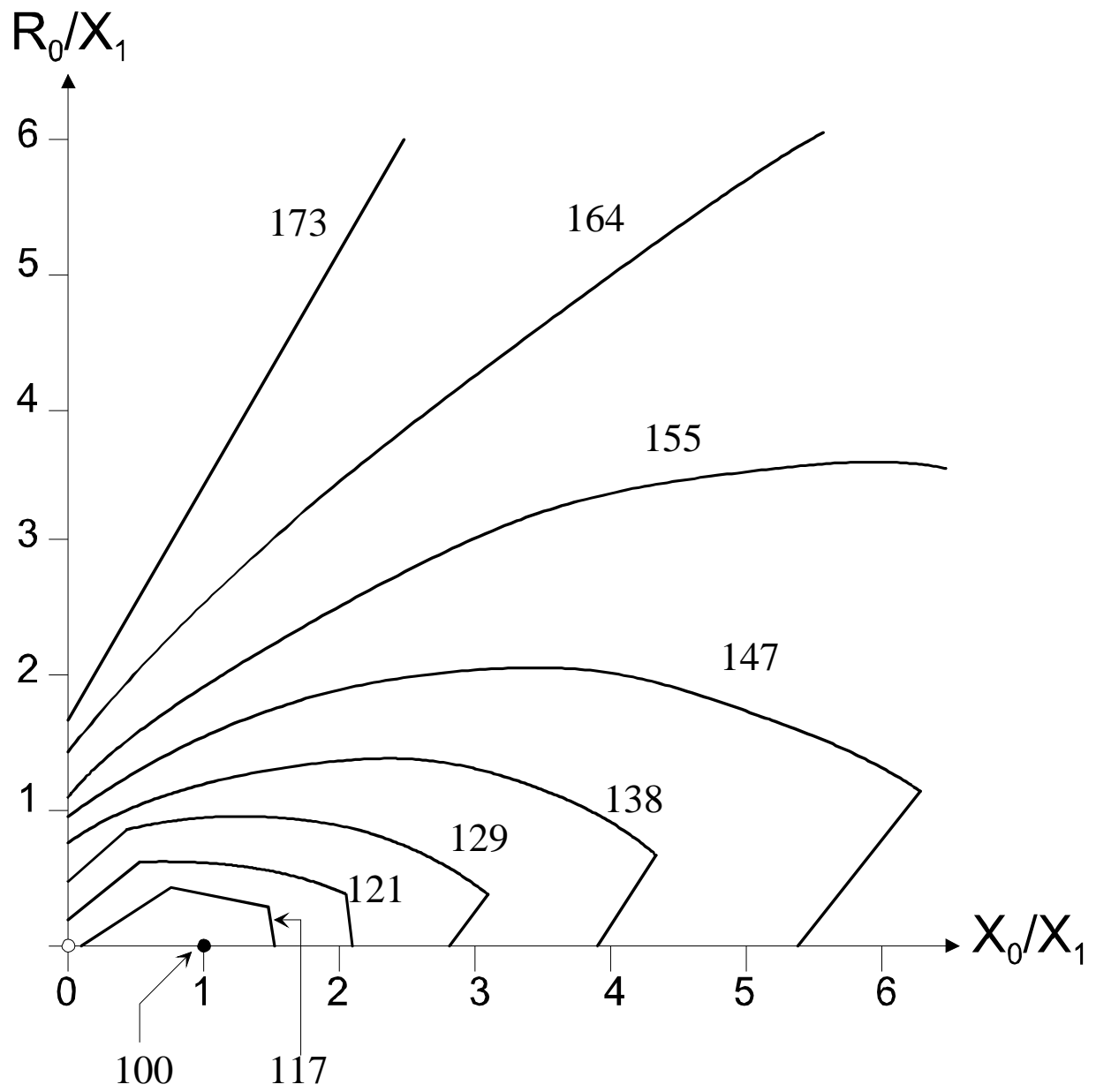


Figure 4.8. Nomogram of Voltage Swells During Single Phase Faults

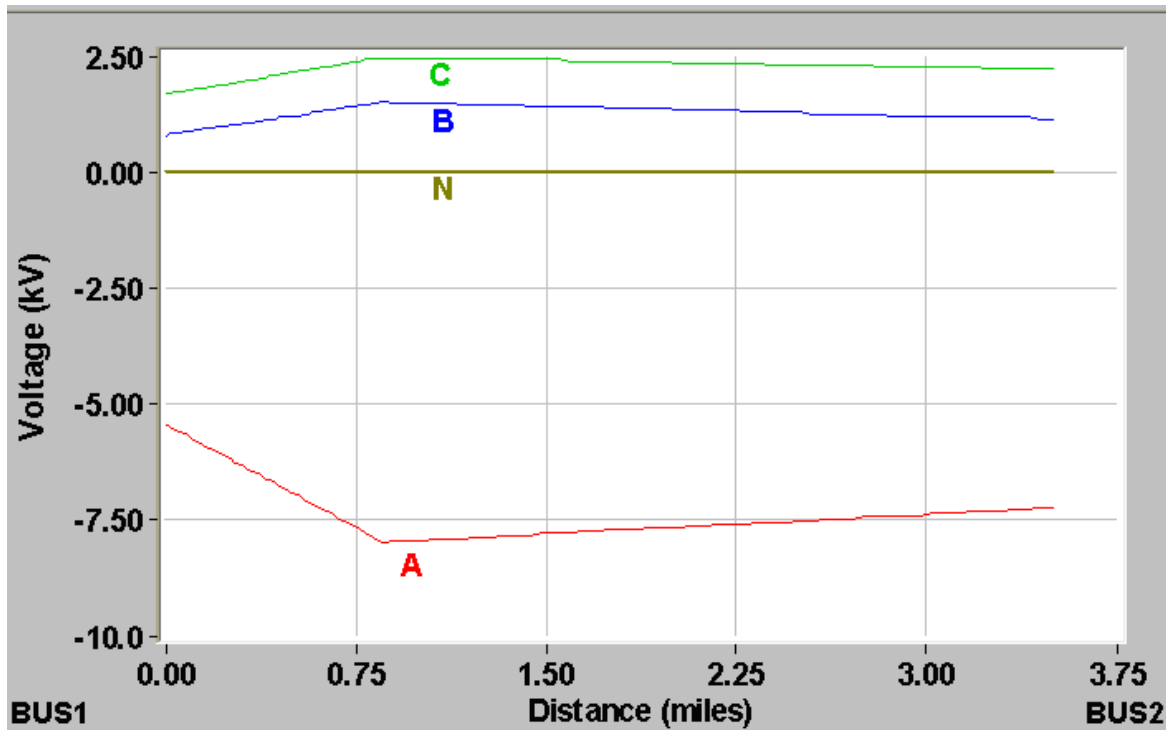


Figure 4.10. Distribution of Voltage Swells and Sags for a Specific Fault Condition and Circuit Design – Deviation from Nominal, Voltages to Neutral

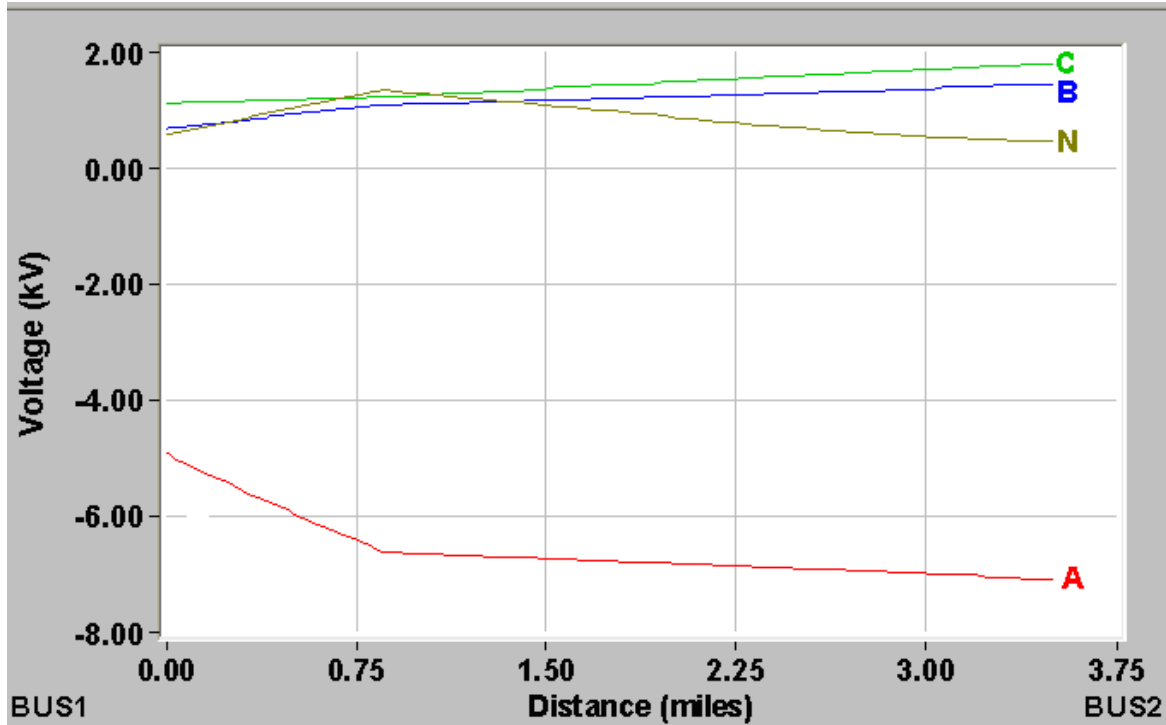


Figure 4.11. Distribution of Voltage Swells and Sags for a Specific Fault Condition and Circuit Design – Deviation from Nominal, Absolute Voltages

What is more important is the statistical distribution of the voltage swells or voltage sags for various types of faults that may occur in the system. This topic is addressed in the section Monte Carlo Simulation.

4.5 Asymmetry and Imbalance

Distribution systems are not symmetric and they are loaded with many single phase loads. Both factors generate unbalanced conditions that can be accentuated with the interaction of dynamic loads such as induction motors. These unbalances can be controlled by appropriate grounding of circuits, use of transformers, placing neutral in symmetric locations with multi-grounds, increasing the size of the neutrals, use of zig-zag transformers, decreasing the impedance of the grounds, etc. The presented model in this paper provides an analytical tool for quantifying the effects of various design options on the unbalance. As an example, Figure 4.12 illustrates an example system that consists of a small section of a typical distribution system with two induction motor loads. One induction motor is directly connected to the distribution system via a cable circuit and the other is connected to the distribution system via a delta-wye connected transformer, solidly grounded on the wye side. This induction motor operates near balanced conditions. The other induction motor, however, is experiencing a rather substantial unbalance, shown in Figure 4.13.

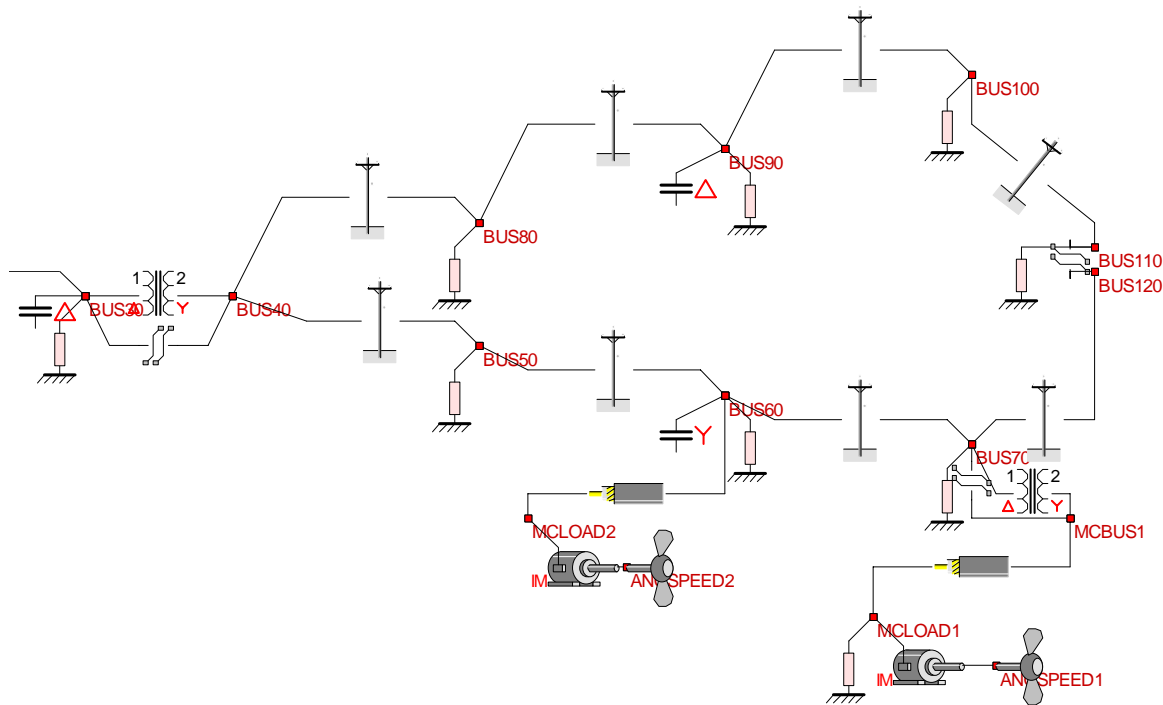


Figure 4.12. Example Distribution System for Unbalance Studies

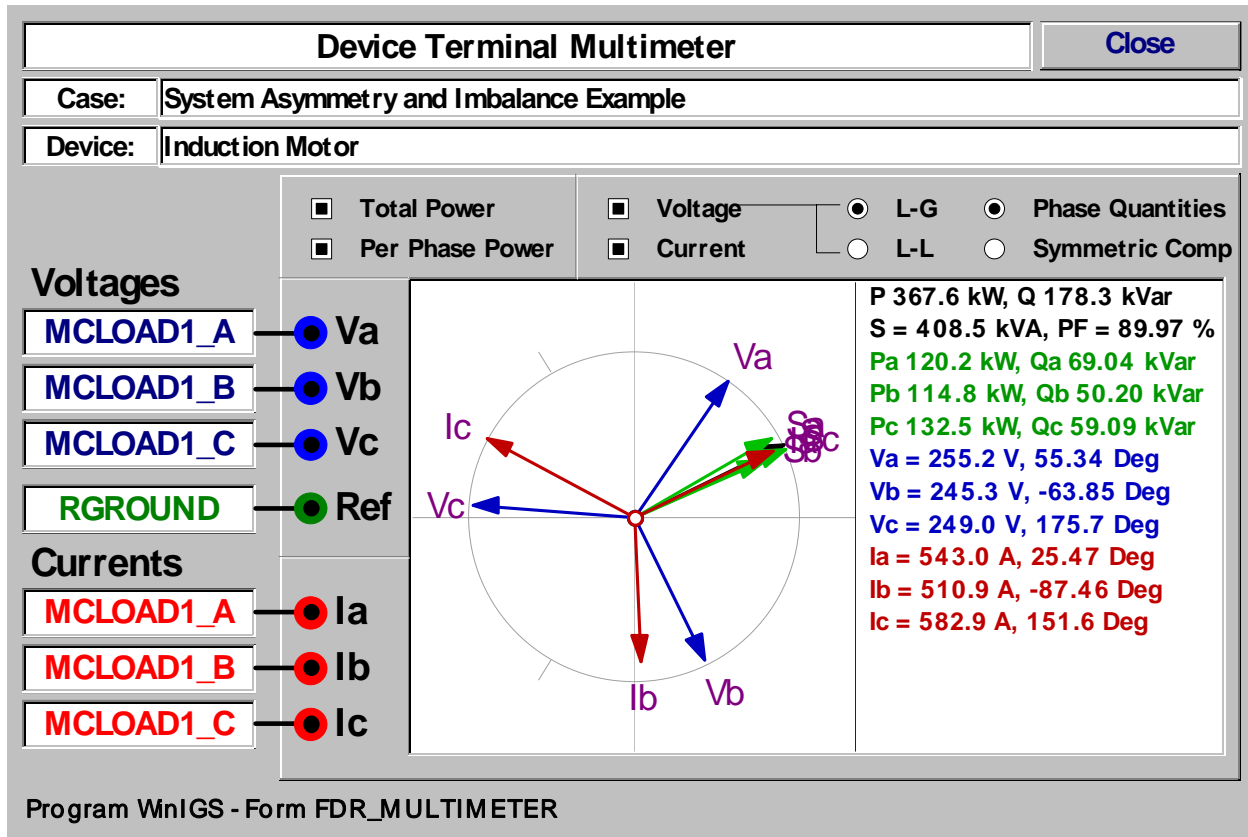


Figure 4.13. Typical Results of Unbalance and Effects on Induction Motors

4.6 Transients Propagation

Switchings and lightning can initiate transients that propagate through the system and reach sensitive customer equipment. The described time domain simulation method computes the transients reaching any point of the system. Thus, the transient voltage waveforms at specific devices terminals are computed and can be compared to the withstand capability (susceptibility curve) of the equipment. This procedure is illustrated in Figures 4.14 and 4.15. Figure 4.14 illustrates the system, the disturbance and the calculation of the transient voltage waveforms. Figure 4.15 illustrates the identification of the frequency and duration content of the waveform and the placement of the disturbance on the susceptibility curve of the equipment. In this way one can determine, by inspection, the effect of the disturbance on the equipment. Note that the computation procedure requires two components: (a) transient voltage computation by means of system-wide disturbance analysis, and (b) characterization of the disturbance at a specific site in terms of frequency content and peak value.

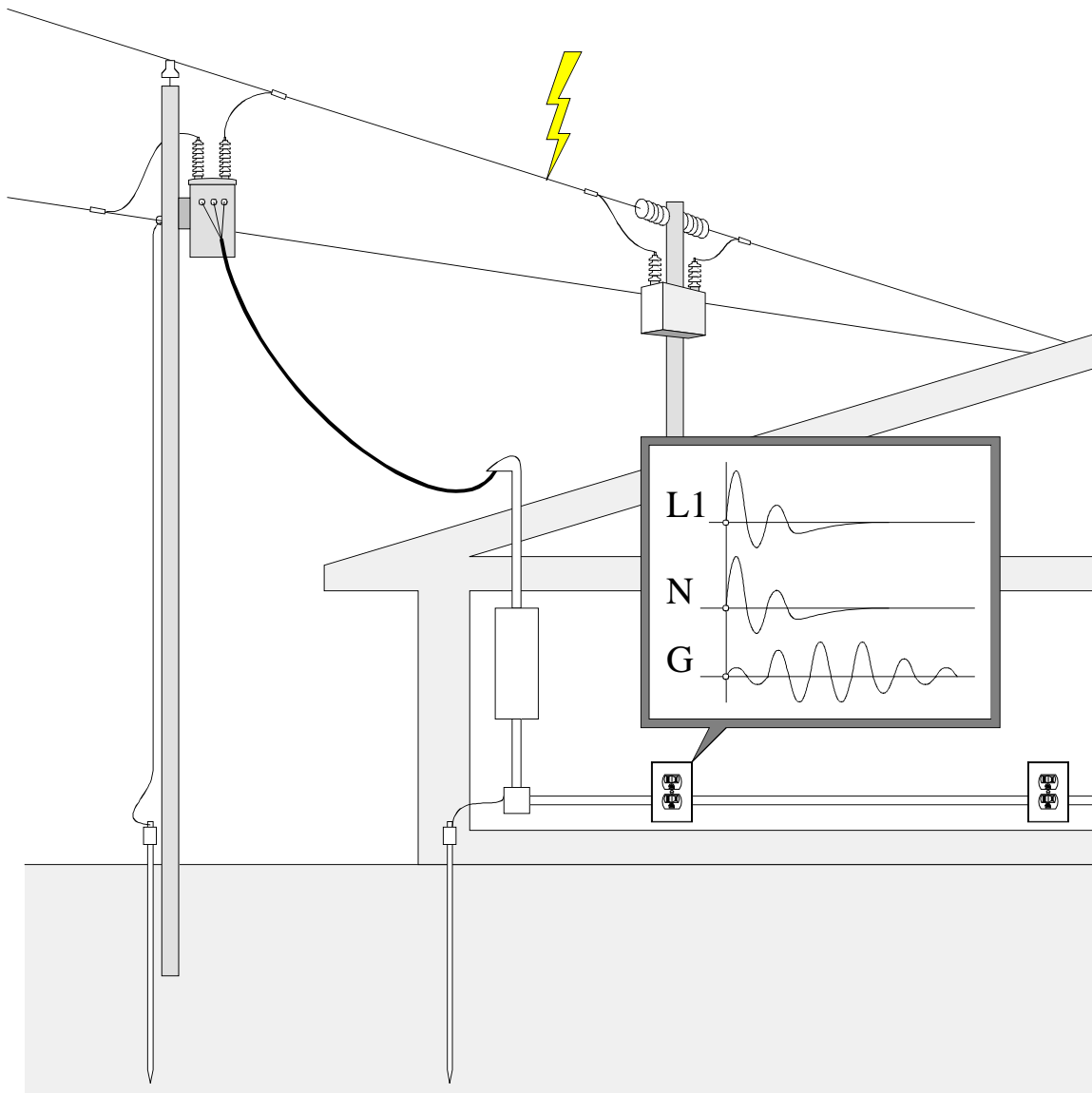


Figure 4.14. Time Domain Simulation of Transient Voltages

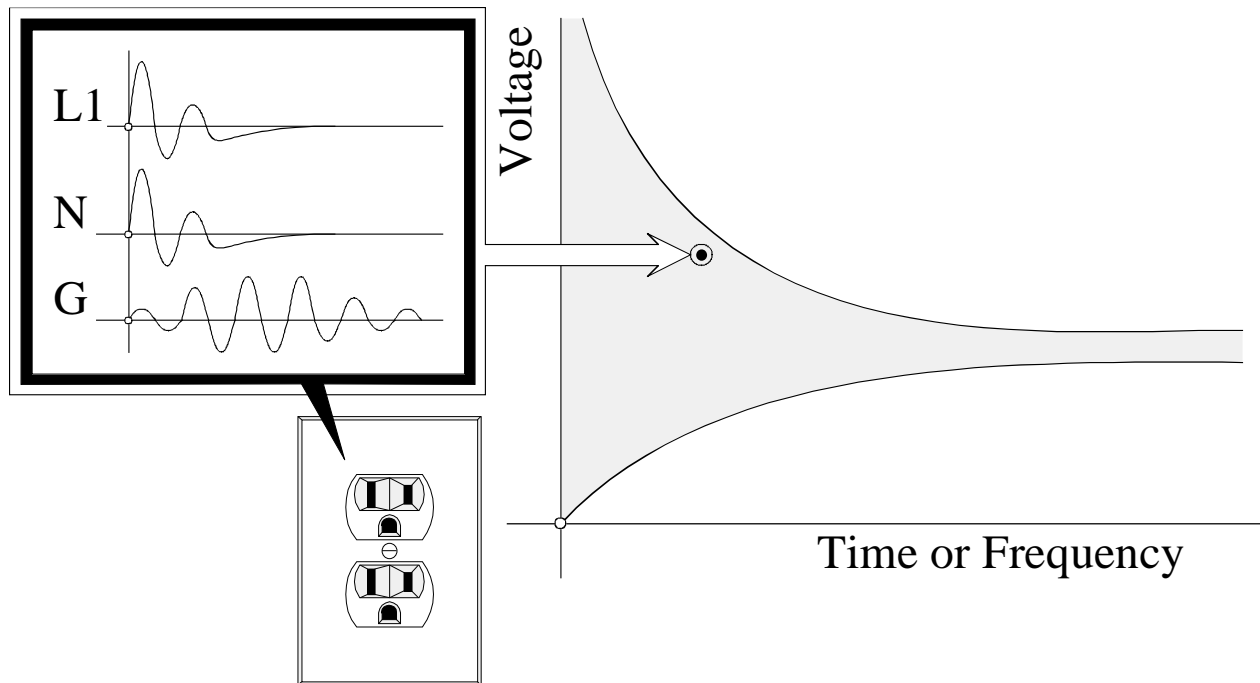


Figure 4.15. Disturbance Characterization Relative to the Susceptibility Curve

4.7 Monte Carlo Simulation

The developed models are used in a Monte Carlo simulation procedure to assess the power quality of the system in a statistical manner. For this purpose, probability distribution functions of random events must be modeled. Then the proposed method consists of the following procedure: first an event is selected (randomly from the known distributions). Then, the condition is simulated and the effects of the condition on power quality are quantified. The procedure is repeated many thousand times and the results are summarized into statistical distribution of maximum overvoltages or current at any selected point in the circuit or as a maximum violation of the susceptibility curve, etc.

The method is applied to two examples. The first example illustrates the application of the method to extract the statistical distribution of voltage sags and swells and the second example provides the distribution of transient voltages due to lightning.

Example 1. The test system of Figure 4.5 has been used to illustrate the computation of voltage sags and swells distribution using a Monte Carlo simulation. For this purpose, an electric fault type is randomly selected (phase A to neutral, Phase A to Phase B, etc), the fault is applied to a randomly selected location of the system (along any circuit) and the condition is simulated to determine the voltage at a specific customer point. The process is repeated many-many times and the results are tabulated into a probability density function, or a cumulative distribution function. Figure 4.16 illustrates the results of this simulation for a customer location at BUS2. Note there is substantial probability for voltage sags in the range (0 to 2 kV) and another substantial

probability for voltage swells in the range (8 kV to 11 kV). Figure 4.17 illustrates the probability density function of the absolute voltages. Note the difference is mainly due to the voltage elevation of the neutral during faults. The proposed model provides a quantitative method to assess this effect.

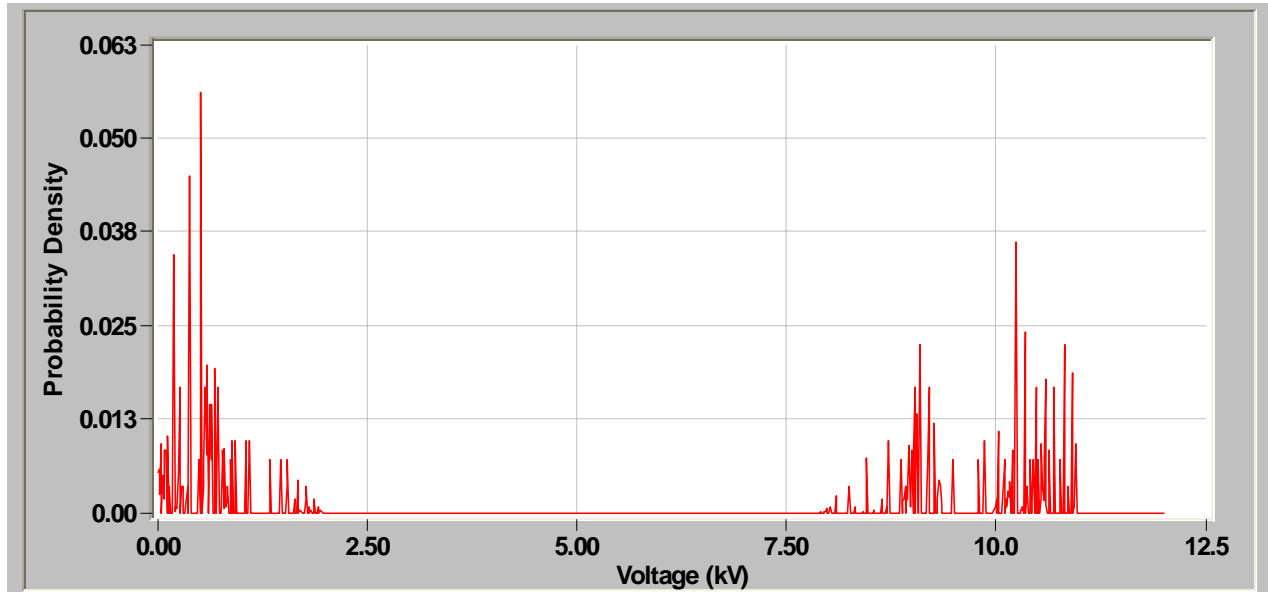


Figure 4.16. Probability Density Function of Voltages (Phase to Neutral) at BUS2

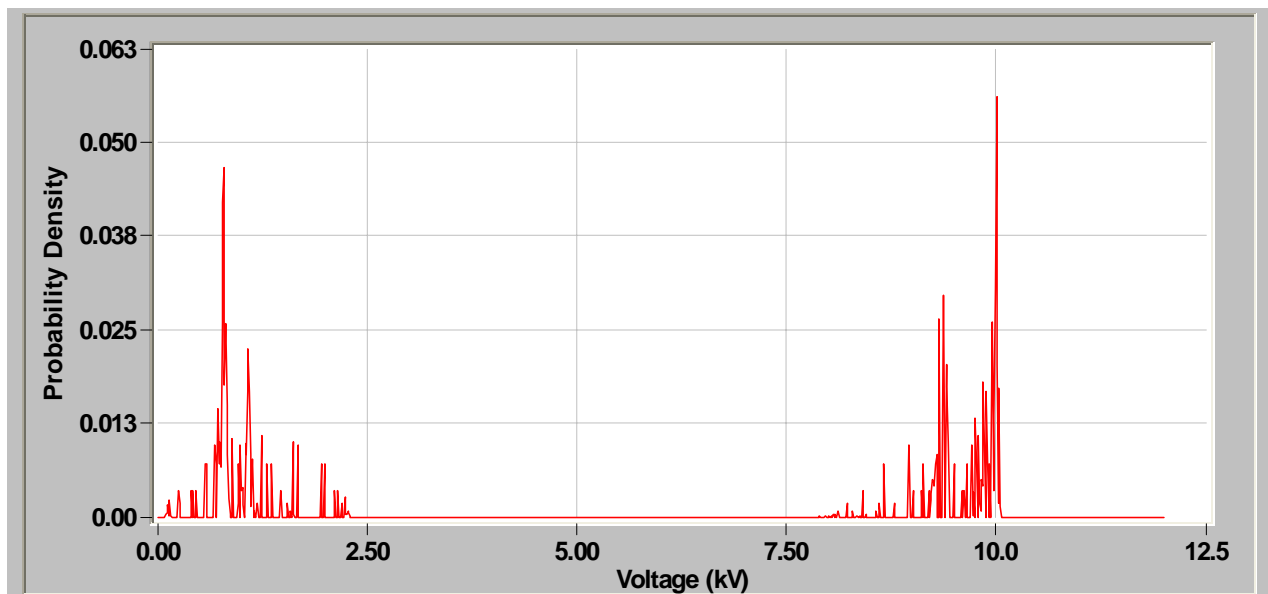


Figure 4.17. Probability Density Function of Voltages (Absolute Voltages) at BUS2

Example 2: Another example system has been used to demonstrate the Monte Carlo simulation approach for assessing lightning overvoltages and their effects on power quality. The system is illustrated in Figure 4.18. The system consists of an industrial facility with electronic equipment. It is fed from an overhead 12 kV distribution circuit via a 0.5 mile underground distribution cable. The facility has a ground loop around the building and the transformer neutral is bonded to the ground loop. The objective of the example is to characterize the disturbances at the terminals of specific electronic equipment.

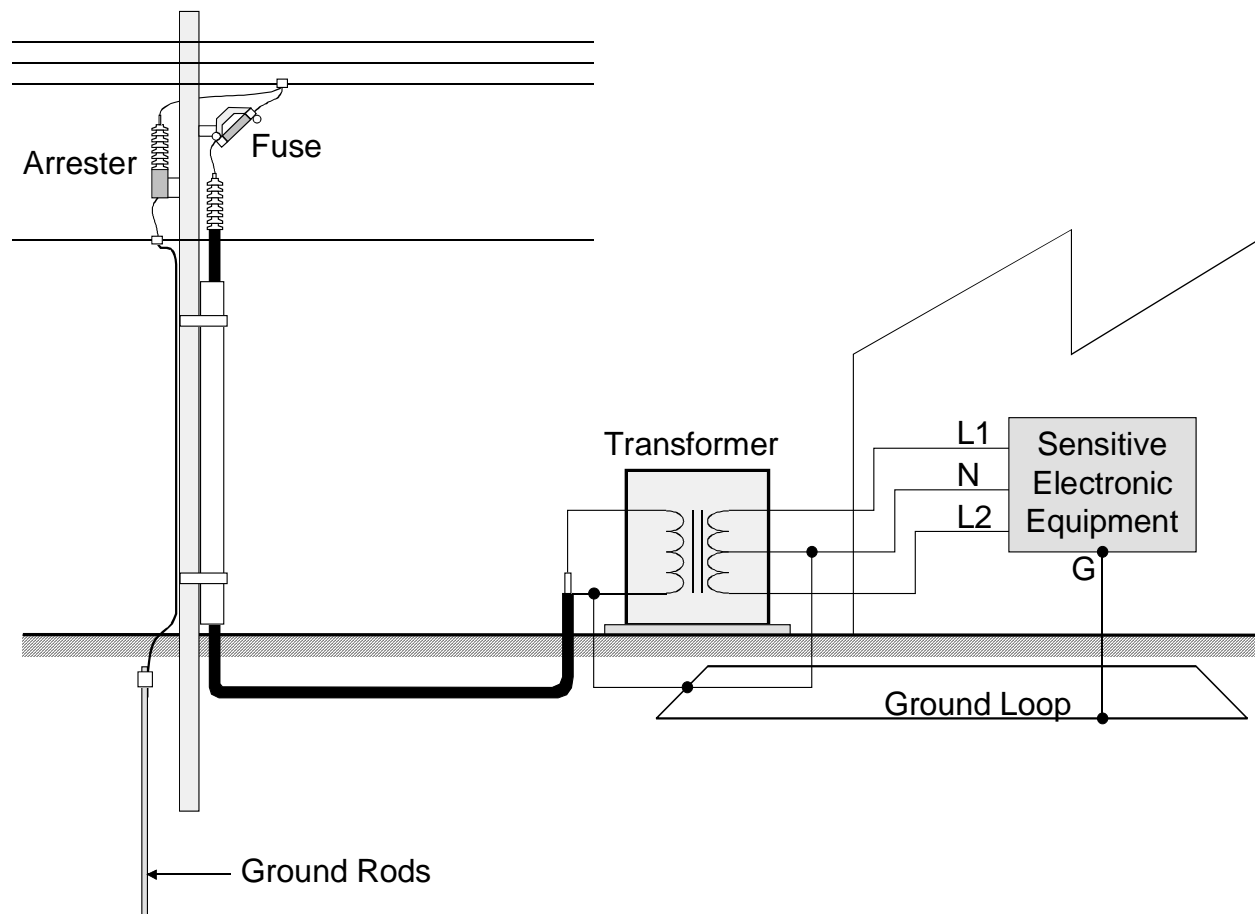
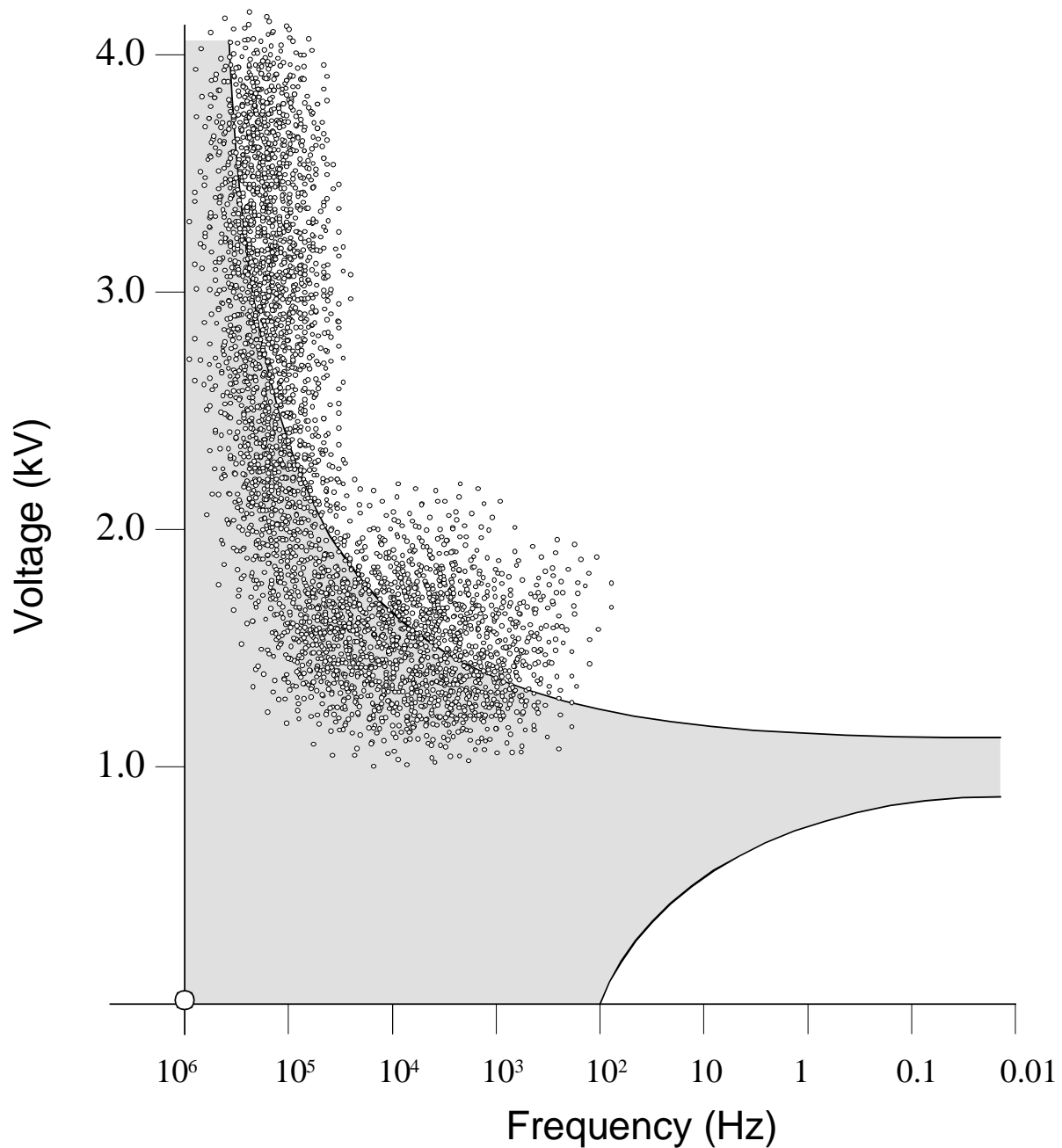


Figure 4.18. Disturbance Characterization Relative to the Susceptibility Curve

The system of Figure 4.18 has been evaluated with a Monte Carlo simulation. Specifically, 5000 trials of lightning and switching disturbances have been simulated and the transients at the terminals of the electronic equipment have been recorded, characterized and superimposed on the susceptibility curve. The results are illustrated in Figure 4.19.



**Figure 4.19. Statistical distribution of Disturbance Voltages
Relative to the Susceptibility Curve**

The results of Figure 4.19 illustrate that there are two clusters of overvoltages, one resulting from lightning and another resulting from switching. The results also provide information on the magnitude of these disturbances as related to the susceptibility of the electronic apparatus. One view of the results of Figure 4.19 is enough to realize that there is a significant number of events that will result in power quality problems for this system. It should be also apparent that the method can be used to assess the effectiveness of specific design modifications on improving the power quality of the system. For example, the grounding of the facility and the 0.5 mile long

cable can be modified (improved) by adding another ground conductor. Then, the Monte Carlo simulation can be repeated. The performance gains then can be assessed and the cost effectiveness of the design modification can be quantified.

5.0 Summary and Conclusions

This report presented physically based modeling and analysis methods of power systems with explicit representation of grounding systems, neutrals and ground wires. The method provides frequency domain solutions as well as time domain solutions. The model can be used to evaluate typical power quality problems on distribution systems. Because the modeling is physically based, one can directly relate design parameters to power quality performance of the system. Application examples have been presented that clearly correlate power quality performance to the design of the system. Low voltage system contains many conduit enclosed circuits. The conduit may be metallic but non-saturable (aluminum) or saturable (steel conduit – EMT, GRC, IMC). Special attention has been given to these circuits. A new modeling methodology has been proposed and implemented. The methodology enables accurate modeling and analysis of these systems.

Typical power quality analysis problems were presented, including harmonic resonance, voltage sags and swells, unbalance, and transients propagation. It is suggested that the best way to use these methods for power quality assessment is to integrate them into a statistical procedure. Monte Carlo simulation provides a good approach for this purpose. The report presented two applications of Monte Carlo simulation for assessing the power quality at specific end-user locations. The applications consider the simulation of a variety of disturbances (i.e., lightning, switching, disturbing loads, faults, etc.). The results are characterized (a) in terms of voltage sags and swells and (b) in terms of frequency and magnitude content and are superimposed on the equipment susceptibility curve. These forms provide useful information about the power quality at a specific end-user site.

The electric power system is continuously evolving. Recent emphasis is in distributed generation. At the same time, most power quality problems are associated with secondary distribution systems; i.e., systems operating at 480 volts or 2x120 volts. Distributed generation has the potential to contribute a fair amount of power quality problems or to provide nice solutions for premium power quality. For example, most newer distributed generation systems are interfaced to the system via power electronic devices that have the capability to provide additional controls to the system, for example to control the level of imbalance in the system and the neutral voltage under normal operating conditions (stray voltages). The presented methodologies address these issues and the associated design problems. We expect that the proposed modeling and analysis methodologies will result in better tools for power quality assessment and improvements in the new complex electric power systems.

In addition to voltage disturbances, one should be concerned with the stability properties of the system, especially the system with distributed energy resources. Of concern is the capability of distributed generation to maintain synchronism under voltage disturbances and a host of other problems. The proposed methodology is a start towards addressing these issues. We plan to explore the applicability of the developed models and methods for studying the stability properties of power distribution systems with distributed energy resources.

6.0 Project-Related Publications

1. A. P. Sakis Meliopoulos, "Impact of Grounding System Design on Power Quality", *IEEE Power Engineering Review*, Vol 21, No. 11, pp 3-7, November 2001.
2. A. P. Sakis Meliopoulos, Elias Glytsis, George J. Cokkinides, Richard Loyd and Patricia Horton, "Grounding and Electromagnetic Analysis of Conduit Enclosed Electric Distribution Systems", *Proceedings of the 2001 IEEE Industrial & Commercial Power Systems Conference*, pp. 157-162, New Orleans, LA, May 13-17, 2001.
3. E. Solodovnik, George J. Cokkinides, Roger Dougal and A. P. Sakis Meliopoulos, "Nonlinear Power System Component Modeling Using Symbolically Assisted Computations", *Proceedings of the 2001 IEEE/PES Summer Meeting*, Vancouver, BC, CN, July 15-19, 2001.
4. A. P. Sakis Meliopoulos, "Distributed Energy Sources: Needs for Analysis and Design", *Proceedings of the 2001 IEEE/PES Summer Meeting*, Vancouver, BC, CN, July 15-19, 2001.
5. A. P. Sakis Meliopoulos, W. Gao and George J. Cokkinides, 'Visualization and Animation of Inverter-Driven Induction Motor Operation', *Proceedings of the 35th Annual Hawaii International Conference on System Sciences*, p. 57 (pp. 1-6), Big Island, Hawaii, January 7-10, 2002.
6. Nikos D. Hatziairgiou and A. P. Sakis Meliopoulos, "Distributed Energy Sources: Technical Challenges", *Proceedings of the 2002 IEEE/PES Winter Meeting*, New York, NY, Jan 28-31, 2002.
7. A. P. Meliopoulos and M. Chen, "A Hybrid Digital Algorithm for Harmonic and Flicker Measurements", *Proceedings of the 2002 IEEE/PES Winter Meeting*, New York, NY, Jan 28-31, 2002.
8. Sakis Meliopoulos, "Challenges in Simulation and Design of μ Grids", *Proceedings of the 2002 IEEE/PES Winter Meeting*, New York, NY, Jan 28-31, 2002.
9. A. P. Sakis Meliopoulos and George J. Cokkinides, *Power Quality Assessment: Status and Needs*, Proceeding of the EMI and PQ Workshop, Atlanta, Georgia, April 18-19, 2002.
10. PhD Thesis: Wengzhong Gao, *A New Methodology for Power System Modeling and Its Application in Machine Modeling and Simulations*, January 2002

7.0 References

1. A. P. Sakis Meliopoulos and G. J. Cokkinides, "A Time Domain Model for Flicker Analysis", *Proceedings of the IPST '97*, pp 365-368, Seattle, WA, June 1997.
2. S. R. H. Hoole, *Computer-Aided Analysis and Design of Electromagnetic Devices*, Elsevier Science Publishing Company, New York 1989.
3. A. P. Sakis Meliopoulos, "Power System Grounding and Transients: An Introduction", Marcel Dekker, New York 1988.
4. Eugene V. Solodovnik, George J. Cokkinides and A. P. Sakis Meliopoulos, "Comparison of Implicit and Explicit Integration Techniques on the Non-Ideal Transformer Example", *Proceedings of the Thirtieth Southeastern Symposium on System Theory*, pp. 32-37, West Virginia, March 1998
5. Eugene V. Solodovnik, George J. Cokkinides and A. P. Sakis Meliopoulos, "On Stability of Implicit Numerical Methods in Nonlinear Dynamical Systems Simulation", *Proceedings of the Thirtieth Southeastern Symposium on System Theory*, pp. 27-31, West Virginia, March 1998.
6. Beides, H., Meliopoulos, A. P. and Zhang, F. "Modeling and Analysis of Power System Under Periodic Steady State Controls", *IEEE 35th Midwest Symposium on Circuit and Systems*
7. IEEE Std 141-1986, IEEE Recommended Practice for Electric Power Distribution for Industrial Plants.
8. IEEE Std 1159-1995, IEEE Recommended Practice for Monitoring Electric Power Quality.
9. IEEE Std 1250-1995, IEEE Guide for Service to Equipment Sensitive to Momentary Voltage Disturbances.
10. ANSI/IEEE Std 519-1981, IEEE Guide for Harmonic Control and Reactive Compensation of Static Power Converters.
11. Eugene V. Solodovnik, George J. Cokkinides and A. P. Sakis Meliopoulos, "Comparison of Implicit and Explicit Integration Techniques on the Non-Ideal Transformer Example", *Proceedings of the Thirtieth Southeastern Symposium on System Theory*, pp. 32-37, West Virginia, March 1998
12. Beides, H., Meliopoulos, A. P. and Zhang, F. "Modeling and Analysis of Power System Under Periodic Steady State Controls", *IEEE 35th Midwest Symposium on Circuit and Systems*
13. IEEE Std 141-1986, IEEE Recommended Practice for Electric Power Distribution for Industrial Plants.
14. IEEE Std 1159-1995, IEEE Recommended Practice for Monitoring Electric Power Quality.
15. IEEE Std 1250-1995, IEEE Guide for Service to Equipment Sensitive to Momentary Voltage Disturbances.
16. ANSI/IEEE Std 519-1981, IEEE Guide for Harmonic Control and Reactive Compensation of Static Power Converters.
17. A. P. Sakis Meliopoulos and G. J. Cokkinides, "A Time Domain Model for Flicker Analysis", *Proceedings of the IPST '97*, pp 365-368, Seattle, WA, June 1997.
18. Eugene V. Solodovnik, George J. Cokkinides and A. P. Sakis Meliopoulos, "Comparison of Implicit and Explicit Integration Techniques on the Non-Ideal Transformer Example", *Proceedings of the Thirtieth Southeastern Symposium on System Theory*, pp. 32-37, West Virginia, March 1998

19. Beides, H., Meliopoulos, A. P. and Zhang, F. "Modeling and Analysis of Power System Under Periodic Steady State Controls", *IEEE 35th Midwest Symposium on Circuit and Systems*
20. IEEE Std 141-1986, IEEE Recommended Practice for Electric Power Distribution for Industrial Plants.
21. IEEE Std 1159-1995, IEEE Recommended Practice for Monitoring Electric Power Quality.
22. IEEE Std 1250-1995, IEEE Guide for Service to Equipment Sensitive to Momentary Voltage Disturbances.
23. ANSI/IEEE Std 519-1981, IEEE Guide for Harmonic Control and Reactive Compensation of Static Power Converters.
24. A. P. Sakis Meliopoulos, "Impact of Grounding System Design on Power Quality", *IEEE Power Engineering Review*, Vol 21, No. 11, pp 3-7, November 2001.
25. Sakis Meliopoulos, "State Estimation for Mega RTOs", *Proceedings of the 2002 IEEE/PES Winter Meeting*, New York, NY, Jan 28-31, 2002.
26. A. P. Sakis Meliopoulos, G. J. Cokkinides and Robert Lasseter, "An Advanced Model for Simulation and Design of Distributed Generation Systems", *Proceedings of MedPower 2002*, Athens, Greece, Nov 3-5, 2002.

Appendix A: Computer Model Description

The work under this project resulted in an improved computer model **GEMI** and a new computer model for distribution system with distributed energy resources, the computer model **μGrid**. Both computer models have an on line help document. In this appendix we present a brief summary of the two computer models.

A.1 Computer Model GEMI

This program performs steady state analysis (short circuit or normal operation) of an electric power system. The program includes detailed models of distribution circuits that take into account the effects of electromagnetic fields such as uneven current distribution, effects of steel conduits including magnetic saturation. Full phase representation is used thus asymmetries due to circuits and single-phase loads are accurately represented. The program output includes plots of magnetic fields along user-selected paths near the network circuits. The program also provides steel, aluminum and PVC conduit design parameters including (see also Figures A-1, A-2):

- Maximum Allowable Steel Conduit Length
- Allowable Length versus Arc Voltage
- Circuit Impedance versus Current
- Magnetic and Field Permeability versus distance from circuit

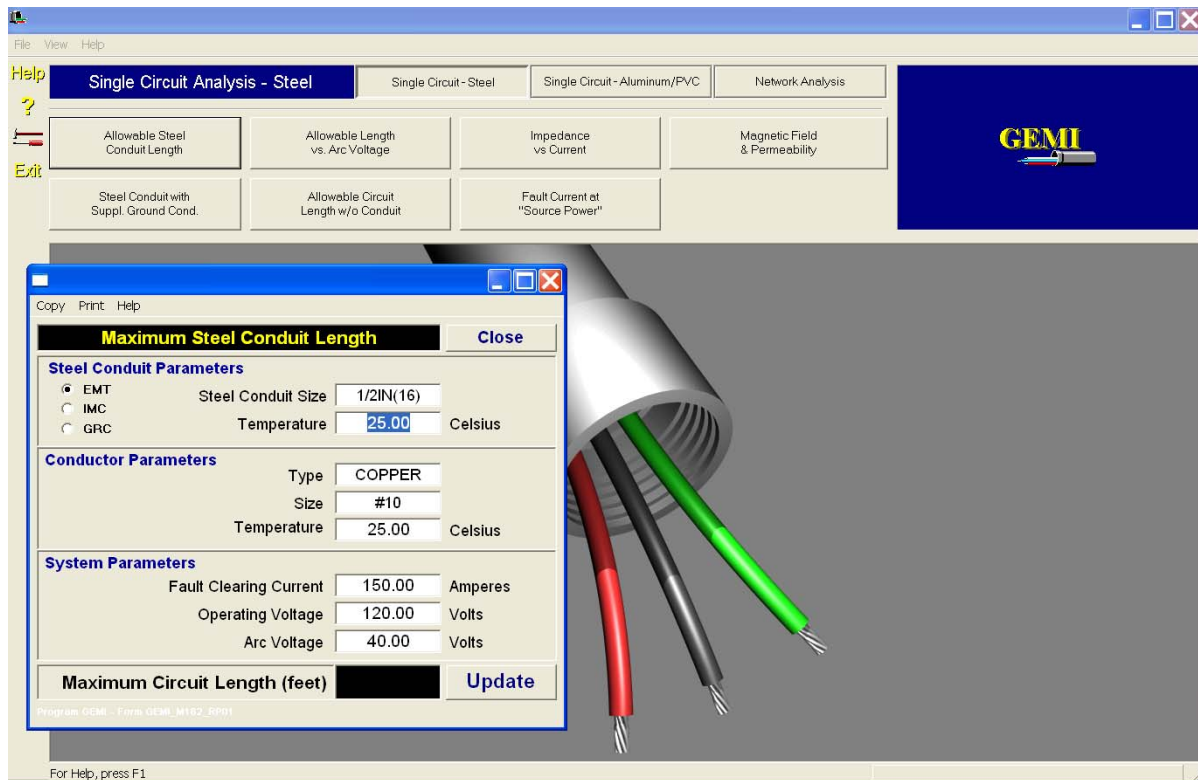


Figure A-1. GEMI Program Single Circuit Steel Conduit Analysis Mode

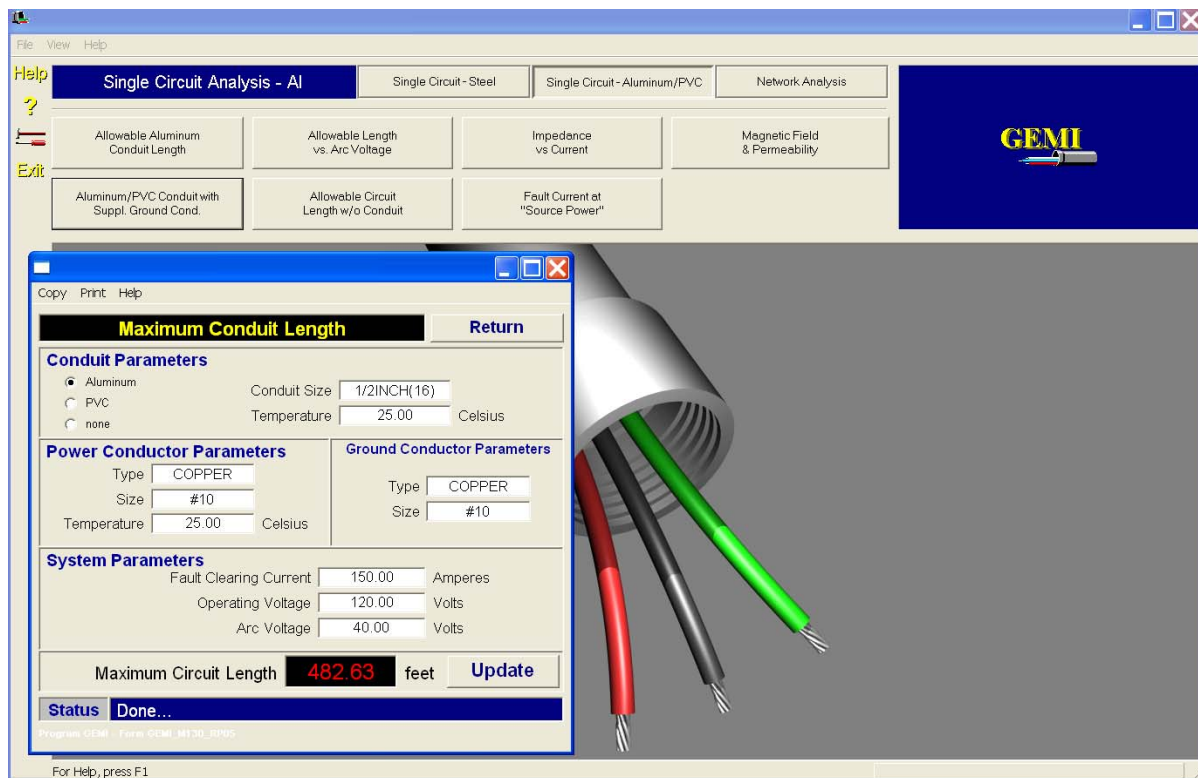


Figure A-2. GEMI Program Single Circuit Aluminum/PVC Analysis Mode

The GEMI program is based on an integrated MS Windows GUI that includes input, analysis, and result-presentation environments. Figure A-3 illustrates the graphical network editor in which the user creates the study network model by graphically manipulating network components in a single line diagram environment. Component parameters are entered via pop-up data entry windows, accessible by a double click on the desired component. For example, Figure A-4 illustrates the input data window for a steel conduit enclosed circuit model. Note that, GEMI circuit models are physically based, and thus require physical input data. Specifically, input data include the conduit and cable conductivity magnetic permeability, dimensions and relative positions. Data entry is simplified by inclusion of cable and conduit libraries containing parameters for most commercially available products. Examples of conduit and cable selection windows are illustrated in Figures A-5 and A-6.

Figure A-7 illustrates a magnetic field report from the same model. The user can graphically or numerically define any path (straight or circular) along which the magnetic field is plotted. Figure A-8 illustrates voltage and current results reported over the network single line diagram.

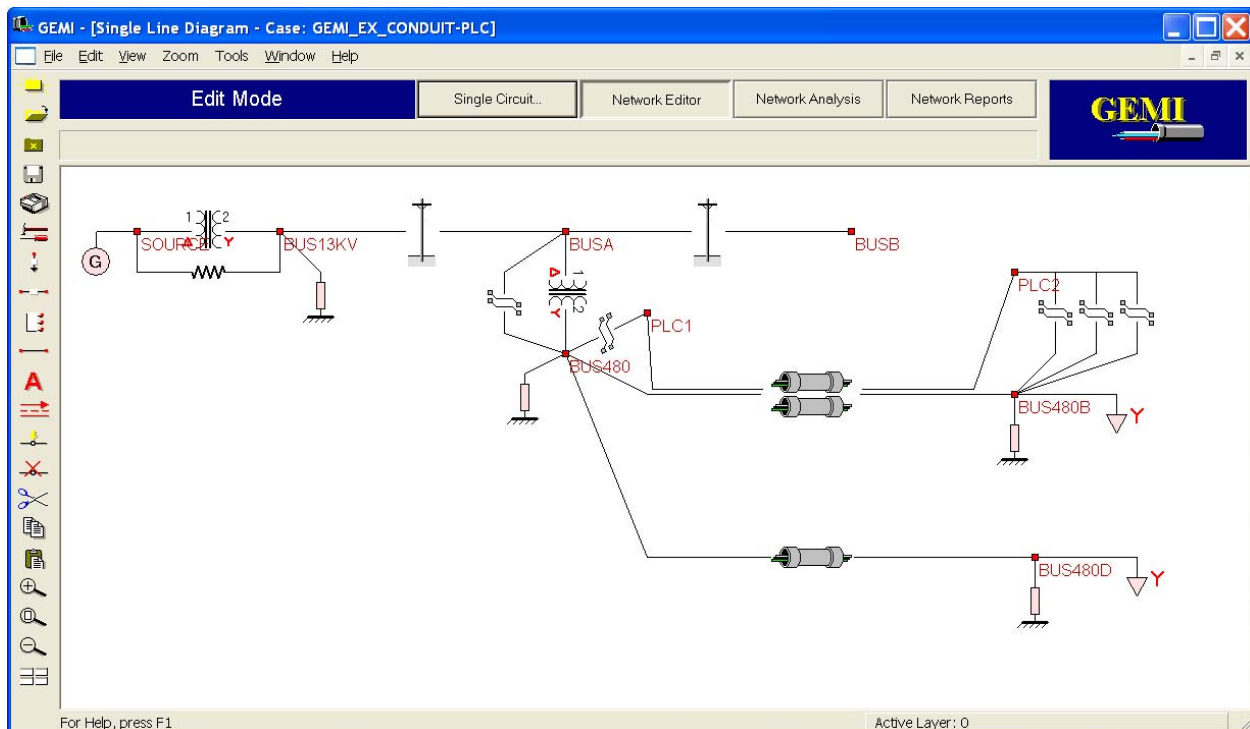


Figure A-3. GEMI Program Network Editor

Copy Print Help

Parallel Steel Conduit Enclosed Circuits

Parallel Steel Conduit and PLC: BUS480 to BUS480B

Accept
Cancel

2.00 inches

Conduits

☒ EMT Copy
☐ IMC Remove
☐ GRC #2 of 2
☐ TROUGH < >

Tmp (C) 25.0
 Size 1/2IN(16)
 Circuit CKT2
 X & Y Coordinates (feet)
 0.4242 1.0082
 Node Name (Side 1) PLC1_N
 Node Name (Side 2) PLC2_G

Conductors

Copy
Remove
#3 of 5 < >

Type COPPER
 Size 3/0
 Circuit CKT1
 X & Y Coordinates (feet)
 0.2517 0.9957
 Node Name (Side 1) BUS480_C
 Node Name (Side 2) BUS480B_C

Circuit Number 1

Circuit Length (feet) 250.0

Soil Resistivity (ohm-meters) 150.0

Redraw
Autoassign Circuits

BUS480_A → BUS480B_A (CKT2)

BUS480_B → BUS480B_B (CKT2)

BUS480_C → BUS480B_C (CKT2)

BUS480_N → BUS480B_G (CKT2)

PLC1_A → PLC2_A (CKT2)

PLC1_B → PLC2_B (CKT2)

PLC1_N → PLC2_G (CKT2)

Program GEMI - Form CODE_163

Figure A-4. GEMI Program Data Entry Form for a Steel Conduit Enclosed Circuit

Copy Print Help

Conduit Library

Cancel
Accept

	Size	Res	Di	Do	Meu
1	EMT				
2	GRC				
3	IMC				
4					
5					
6					
7					
8					
9					
10					
1	1/2IN(16)	3.9536	0.6220	0.7060	1300.0
2	3/4IN(21)	2.5775	0.8240	0.9220	1300.0
3	1INCH(27)	1.7489	1.0490	1.1630	1300.0
4	1-1/4IN(35)	1.1739	1.3800	1.5100	1300.0
5	1-1/2IN(41)	1.0127	1.6100	1.7400	1300.0
6	2INCH(53)	0.7956	2.0670	2.1970	1300.0
7	2-1/2IN(63)	0.5463	2.7310	2.8750	1300.0
8	3INCH(78)	0.4467	3.3560	3.5000	1300.0
9	3-1/2IN(91)	0.3391	3.8340	4.0000	1300.0
10	4INCH(103)	0.3007	4.3340	4.5000	1300.0

Program GEMI - Form LBE_004

Figure A-5. GEMI Conduit Selection Window

Copy Print Help

Conductor Library

Accept Cancel

Sort by Name Sort by Size

	AWG	Metric	DCRes	Area	Dia
13	2/0	N/A	0.4277	133.10	0.4180
14	3/0	N/A	0.3389	167.80	0.4700
15	4/0	N/A	0.2693	211.60	0.5280
16	250KCM	N/A	0.2276	250.00	0.5750
17	300KCM	N/A	0.1901	300.00	0.6300
18	350KCM	N/A	0.1626	350.00	0.6810
19	400KCM	N/A	0.1420	400.00	0.7280
20	500KCM	N/A	0.1140	500.00	0.8130
21	600KCM	N/A	0.0950	600.00	0.8930
22	700KCM	N/A	0.0813	700.00	0.9640
23	750KCM	N/A	0.0760	750.00	0.9980
24	800KCM	N/A	0.0713	800.00	1.0300
25	900KCM	N/A	0.0634	900.00	1.0940
26	1000KCM	N/A	0.0570	1000.00	1.1520
27	1250KCM	N/A	0.0456	1250.00	1.2890
28	1500KCM	N/A	0.0379	1500.00	1.4120

Resistance in ohms/mile, area in cmils, diameter in inches.

Program GEMI - Form LBE_001

Figure A-6. GEMI Cable Selection Window

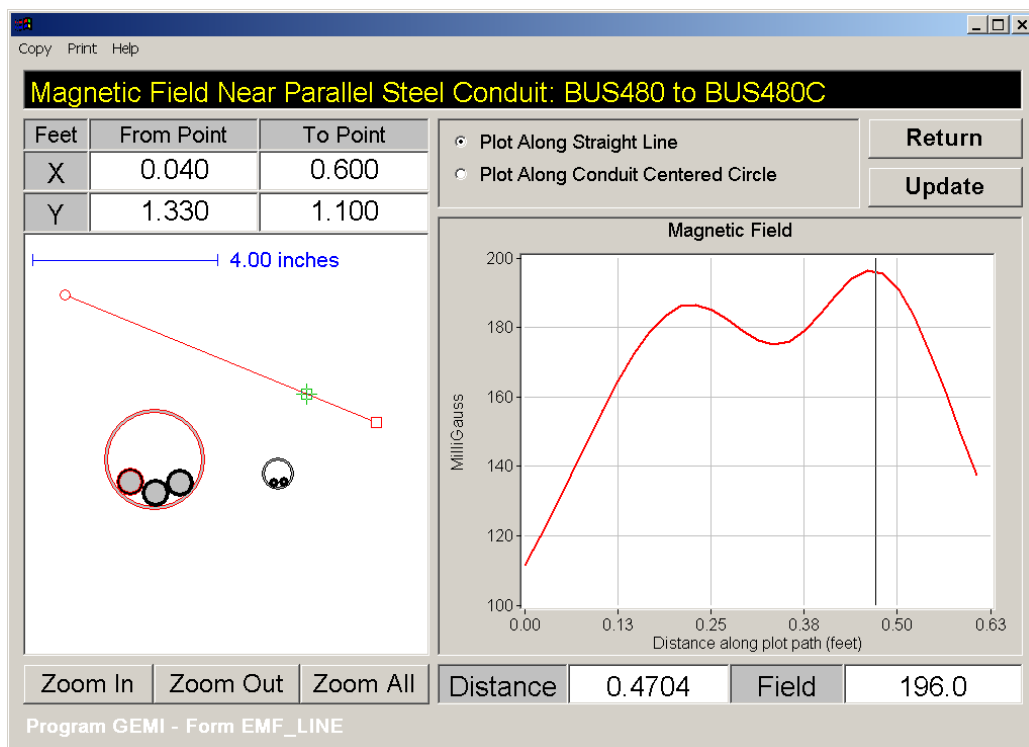


Figure A-7. GEMI Program Magnetic Field Report Form for a Steel Conduit Enclosed Circuit

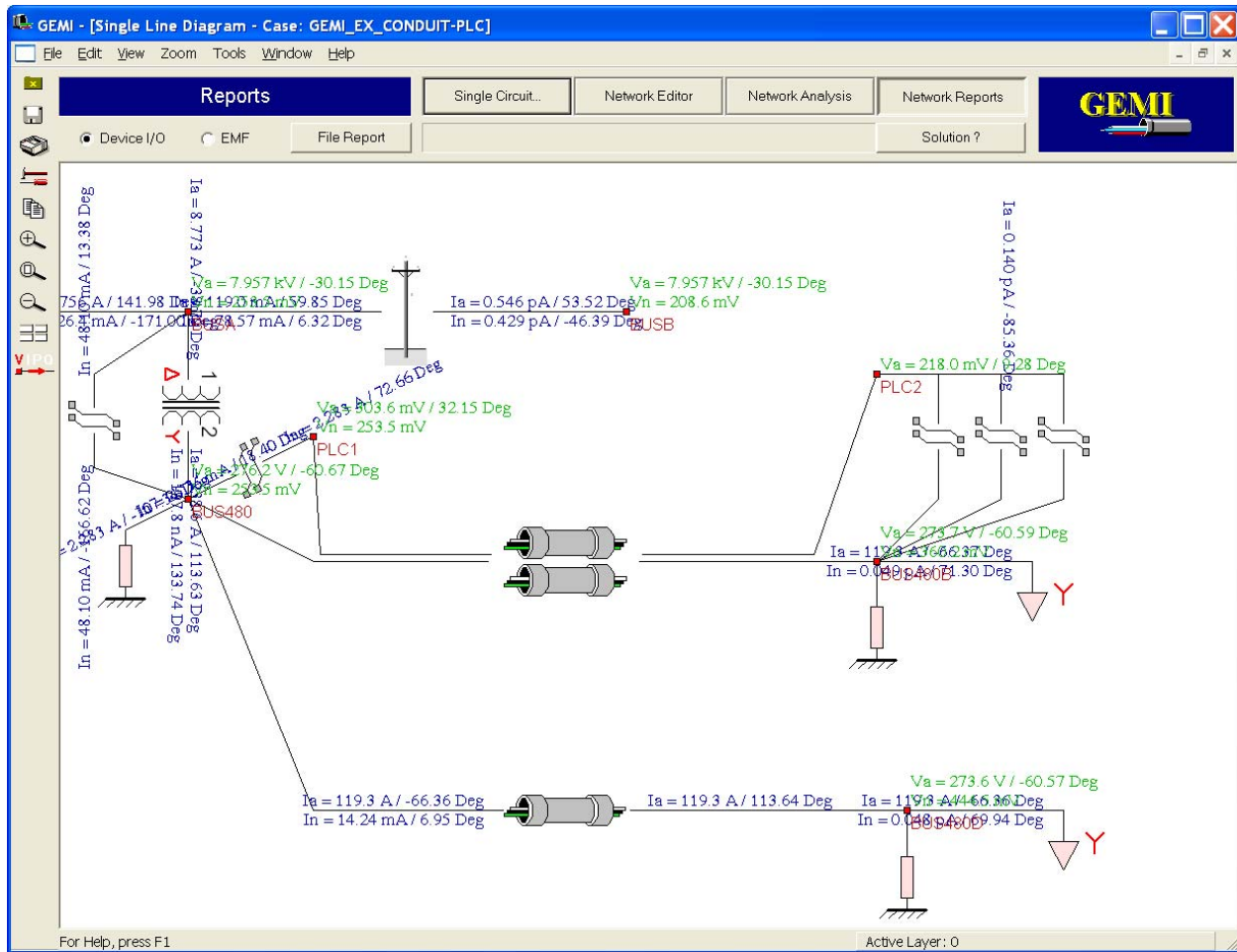


Figure A-8. GEMI Program Results Display View

A.2 Computer Model μ GRID

This program is suitable for analysis of micro-grids and the study of the effects of asymmetries and unbalances on such systems. It is based on a general method for large-scale multiphase power flow analysis with the following unique characteristics: (a) each system component is modeled in direct phase quantities and without any approximating assumptions, such as balanced voltages and currents or symmetric network components, (b) the model is quadratized; (i.e., any nonlinear model of a system component is converted into a set of second order equations with the introduction of appropriate transformations, and (c) the method introduces the composite node concept, which enables efficient application of sparsity techniques, optimal ordering, LU decomposition and forward and back substitution. The solution method of the overall model is based on Newton's method. Since the model is quadratized, Newton's method provides fast convergence (quadratic).

The modeled system may include any number of symmetric three phase devices as well as asymmetric elements. Presently the program supports power systems comprising any combination of devices including:

- Various types of micro-Sources (micro-turbines, fuel cells, inverters etc.)
- Transmission and Distribution lines
- Transformers
- Loads

The μ GRID program organization is similar to GEMI, as it includes seamlessly integrated input, analysis, and result-presentation environments. Figure A-9 illustrates the μ GRID network editor displaying a typical μ GRID system.

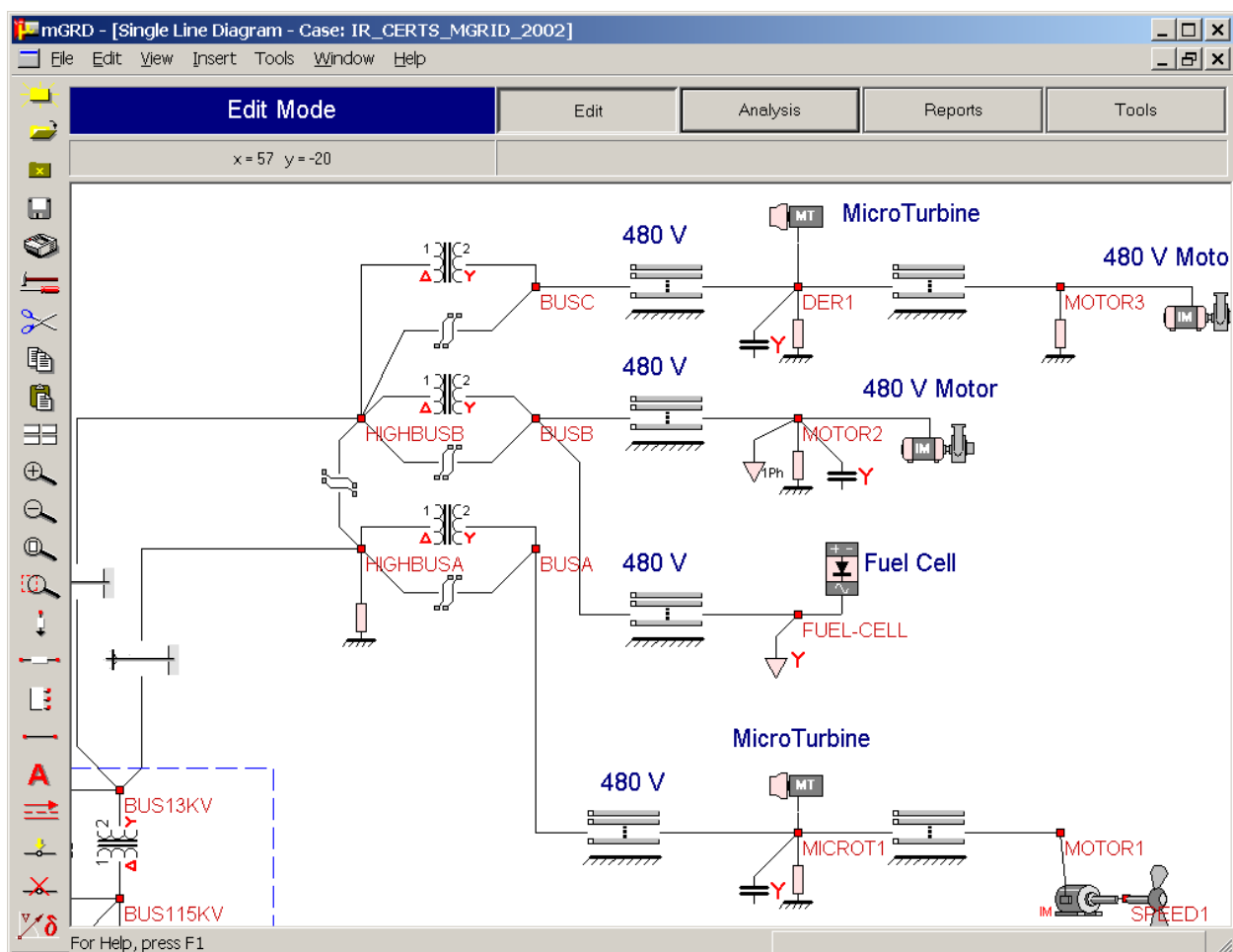
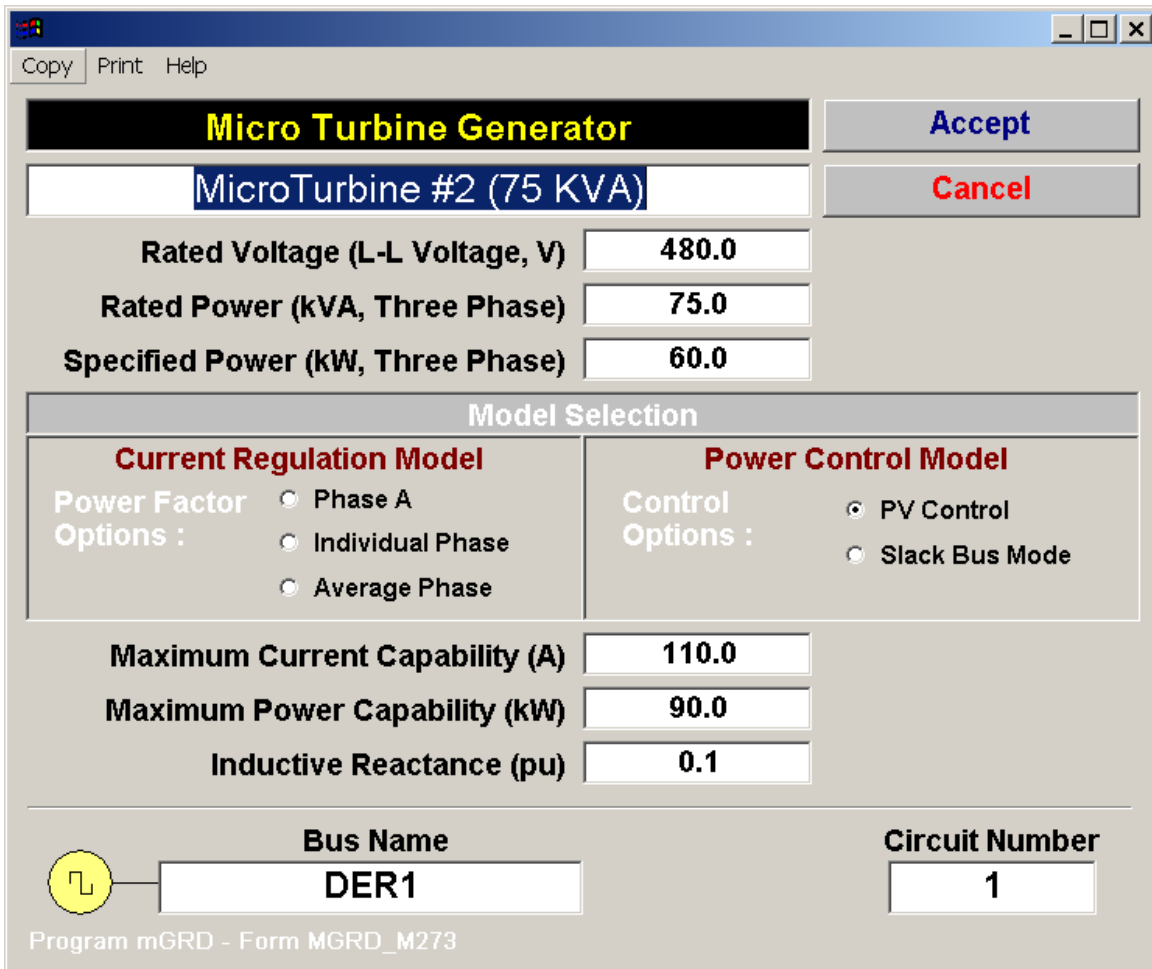


Figure A-9. μ GRID Program Network Editor

Figure A-10 illustrates the data entry form for a microturbine generator model. Note that the input data include several control options; i.e., current, real power, voltage, slack bus mode, etc.

Once the solution is completed, reports of voltages, currents, power flows, etc are selectively generated via interaction with the system single line diagram. Figure A-11 illustrates the

Multimeter report window showing the voltages, currents, and power output of a microturbine-generator.



Micro Turbine Generator

MicroTurbine #2 (75 KVA)

Rated Voltage (L-L Voltage, V) 480.0

Rated Power (kVA, Three Phase) 75.0

Specified Power (kW, Three Phase) 60.0

Model Selection

Current Regulation Model

Power Factor Options :

- ☐ Phase A
- ☐ Individual Phase
- ☐ Average Phase

Power Control Model

Control Options :

- ☒ PV Control
- ☐ Slack Bus Mode

Maximum Current Capability (A) 110.0

Maximum Power Capability (kW) 90.0

Inductive Reactance (pu) 0.1

Bus Name DER1

Circuit Number 1

Program mGRD - Form MGRD_M273

Figure A-10. Microturbine Model Data Entry Form

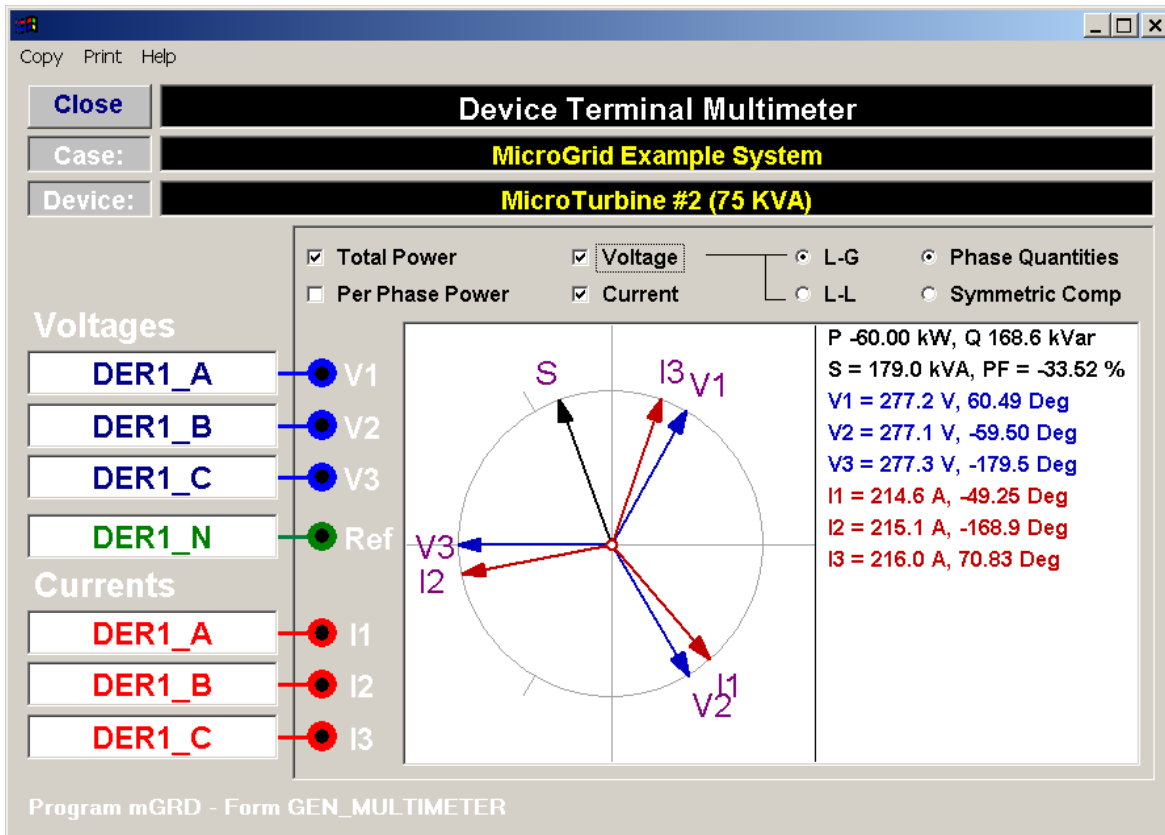


Figure A-11. Multimeter Tool Displaying Microturbine Operating State